1

AGB Stars in Binaries and Their Progeny

1 The Binary–AGB Connection

Although binarity and AGB evolution are in principle disconnected concepts (a star need not be member of a binary system to evolve along the AGB), a rich world flourishes at their contact. The interest in discussing binary stars with an AGB component goes far beyond the possibility of deriving their masses. First, binarity is expected to alter the intrinsic properties of AGB stars (pulsation, mass loss, dust formation, etc.). Second, the importance of the rich progeny of binary stars involving AGB stars has been recognized recently. Various classes of stars with peculiar abundances (such as barium stars, CH stars, Tc-poor S stars, etc.) have indeed been identified as the progeny of binary systems formerly involving an AGB star. Mass transfer from the AGB component is held responsible for the chemical anomalies now observed at the surface of the companion star, which dominates the light of the system, since the AGB star has evolved into a dim white dwarf (WD). Therefore, two broad classes of binary systems must be distinguished in relation to AGB stars: (A) The primary star[1] is currently an AGB star, while the secondary is still an unevolved dwarf; (B) The secondary is a WD, while the primary is at any evolutionary stage (except WD) and has been polluted by the secondary when the latter was an AGB star.[2] The present chapter is organized as follows. Sections 2 and 3 deal with case A. They present, respectively, a brief review

[1] Defined as the star dominating the visible spectrum.

[2] The case in which both stars are simultaneously on the AGB is expected to be rare, given the short time scale of the AGB evolution with respect to the total stellar lifetime. Such systems require that the two stars had initial masses differing by a very small amount. Recent discussions of the distribution of initial mass ratios q in binary systems (see the contributions by Mayor et al., by Tokovinin, and by Larson in IAU Symposium 200 *The Formation of Binary Stars*) reveal that the case $q = 1$ is not especially frequent among binaries with periods larger than about 100 d, which are those relevant to the present discussion. Systems consisting of two AGB stars need not therefore be further discussed here.

of the (poor) statistics of binaries among AGB stars, and of the impact of binarity on various properties of AGB stars. Section 4 deals with case B. Section 4.1.1 addresses the question of distinguishing systems belonging to cases A and B when the primary is a giant. Section 4.2 then enumerates the various families of peculiar stars belonging to case B. Section 4.3.1 reviews their orbital properties, while Section 4.4 shows how these orbital properties make it possible to set constraints on the mass-transfer mode that took place in those systems.

2 AGB Stars in Binary Systems

2.1 Constraints on the Properties of Binary Systems Involving AGB Stars

Before discussing the methods available for identifying binary systems involving AGB stars (Section 2.2), it is interesting first to evaluate how the very large size of AGB stars sets a lower bound on the orbital separation—and hence on the orbital period—through the concept of the critical Roche radius.

2.1.1 Roche Radius

In the Roche description of a binary system (following the French physicist E. Roche 1820–1883), it is assumed that the gravitational fields of the two stars can be approximated by those of two point masses, that the orbits are circular, and that the two stars are in synchronous rotation with the orbital motion (so-called corotation). Under these conditions, the binary system appears to be at rest in a frame corotating with the orbital motion. In this frame, it is possible to define effective equipotential surfaces corresponding to the gravitational potential corrected for centrifugal effects due to the rotation of the frame (for a detailed description of the Roche model, see [68]). Equipotential surfaces are surfaces of constant Φ, where

$$\Phi = -\frac{\tilde{\mu}}{r_1} - \frac{1-\tilde{\mu}}{r_2} - \frac{x^2+y^2}{2}, \tag{1}$$

with $\tilde{\mu} = M_1/(M_1+M_2)$, and $r_1 = [(x+1-\tilde{\mu})^2 + y^2 + z^2]^{1/2}$ is the distance to the star of mass M_1 lying at $(\tilde{\mu}-1, 0, 0)$, $r_2 = [(x-\tilde{\mu})^2 + y^2 + z^2]^{1/2}$ the distance to the star of mass M_2 lying at $(\tilde{\mu}, 0, 0)$, so that the center of mass corresponds to the origin of the coordinate system, and the orbital plane is the xy–plane. In (1), distances are expressed in units of the orbital separation, time is expressed in units of the orbital period, and masses in units of (M_1+M_2). The most important equipotential surface, from the point of view of binary-star evolution, is the critical surface whose intersection with the orbital plane forms a figure eight (Figure 1). The two cusped volumes that are enclosed by this critical surface are called the Roche lobes of the respective stars. They have a single contact point, along the line joining the two stars, called the inner Lagrangian point, usually denoted by L_1 and corresponding to the point located between the two stars where $\mathrm{d}\Phi/\mathrm{d}x = 0$. A system in which both components are within their Roche lobes is called *detached*. If one component fills its Roche lobe, the system is called *semidetached*, and when both components overflow their Roche lobes, the system is called a *contact* binary (Figure 1). Mass transfer occurs from the Roche-filling star to its companion in semidetached systems, and this phenomenon is usually referred to as *Roche lobe overflow* (RLOF). When involving an AGB star more massive than its companion, RLOF is usually considered to be dynamically unstable, and to lead to dramatic orbital shrinkage through a common envelope (CE) phase. Although this general statement will be somewhat attenuated in the detailed discussion presented in Section 4.4, it is nevertheless clear that the size of the Roche lobe constitutes a physical limit to the size that may be reached by an AGB star in a binary system. Conversely, knowing the size of an AGB star, it is possible to set a lower limit on the orbital separation of the binary system that is able to host it.

A useful approximation of the Roche radius, corresponding to the radius of the sphere having the same volume as the Roche lobe surrounding star 2, is given by (e.g., [68])

$$R_{R,2}/A = \begin{cases} 0.38 + 0.2 \log q, & 0.5 \leq q \leq 20, \\ 0.462 \left(\frac{q}{1+q}\right)^{1/3}, & 0 < q < 0.5, \end{cases} \tag{2}$$

where $q = M_2/M_1$, and A is the orbital separation. An alternative expression, valid for all q, is

$$R_{R,2}/A = \frac{0.49\, q^{2/3}}{0.6\, q^{2/3} + \ln(1 + q^{1/3})}. \tag{3}$$

2.1.2 Limitations of the Roche Lobe Concept in the Case of AGB Stars

The validity of the Roche approximation for mass-losing AGB stars has to be questioned in several respects. The Roche model described in Section 2.1.1 assumes that the two stars are point masses (a good approximation for centrally condensed objects like AGB stars), and that the only forces acting upon a test mass corotating with the binary system are the centrifugal pseudo-force and the gravitational forces of the two point-like stars. In particular, the radiation pressure and the shock waves imparting momentum on the escaping matter (from a reservoir of internal energy), as is the case for AGB winds, are not included in the Roche model. Therefore, the very concept of Roche lobe may be irrelevant for systems involving a mass-losing star where the wind-driving force may substantially reduce the effective gravity of the mass-losing star. Since both the radiation-pressure force ($\mathrm{d}P_r/\mathrm{d}r$) on the wind and the gravitational attraction decrease as r_2^{-2}, where r_2 is the distance to the AGB star,

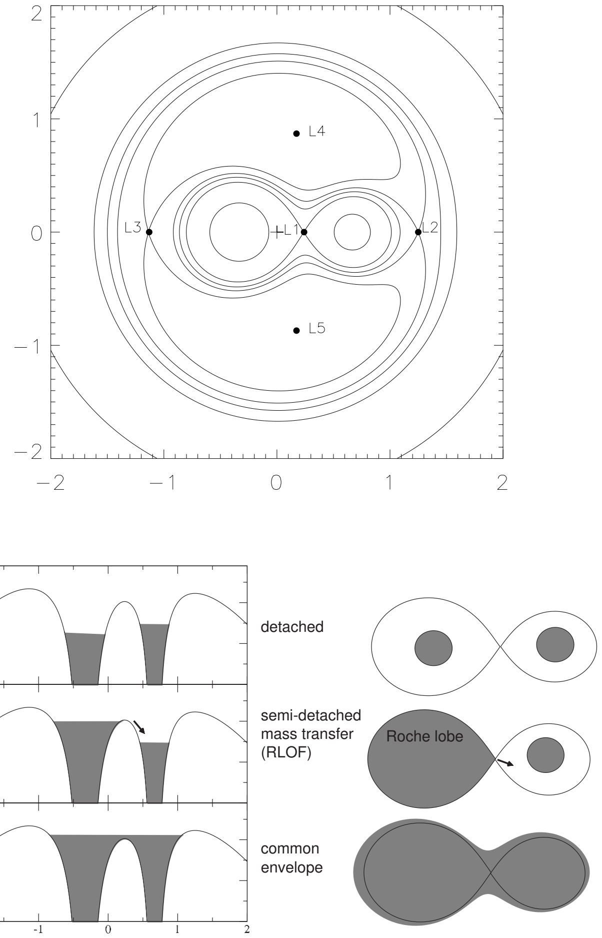

Fig. 1. Top panel: Sections in the orbital plane of Roche equipotentials, for a binary system with mass ratio $q = M_2/M_1 = 0.5$. The position of the Lagrangian point L_1 (black dot) is indicated, as well as that of the center of mass (cross) of the system.
Bottom panel: A schematic representation of the equipotentials as a function of distance along the line joining the two stars: **(top panel)** detached binary; **(middle panel)** semi-detached binary; **(bottom panel)** contact binary.

the net effect on the wind particle may be seen as a reduction of the effective gravity of the AGB star by the factor $(1 - f)$, where f is the ratio of the radiation pressure force per unit mass to the gravitational attraction (per unit mass) of the AGB star at any given point:

$$f = \frac{-\mathrm{d}P_r}{\rho\,\mathrm{d}r}\left(\frac{GM_2}{r_2^2}\right)^{-1}, \tag{4}$$

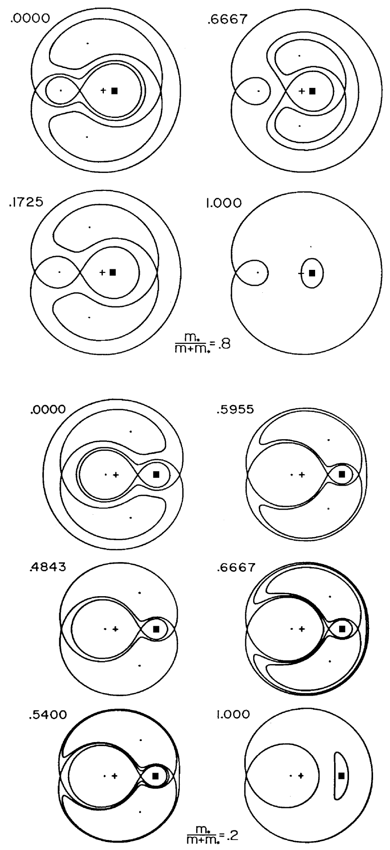

Fig. 2. Modification of the Roche equipotentials in the presence of an extra force driving the mass loss from star 2 (represented by a filled square symbol). The **upper four** correspond to $1 - \tilde{\mu} = 0.8$ and the six **lower panels** to 0.2, respectively. The various figures correspond to different f values, as labeled (with $f_c = 0.1725$ in the four **upper panels** and 0.5955 in the six **lower panels**). Compare with Figure 1. From [120].

or

$$f \equiv \frac{1}{4\pi c G M_2} \int_0^\infty \kappa_\nu \, L_{\nu,2} \, \mathrm{d}\nu, \tag{5}$$

since the radiation pressure force can be written

$$\frac{\mathrm{d}P_r}{\mathrm{d}r} = -\frac{1}{c} \int_0^\infty \kappa_\nu \, \rho \, \frac{L_{\nu,2}}{4\pi r_2^2} \, \mathrm{d}\nu, \tag{6}$$

where κ_ν is the absorption coefficient per unit mass at frequency ν, c the speed of light, and $L_{\nu,2}$ the luminosity of star 2 in the frequency range $(\nu, \nu+\mathrm{d}\nu)$. The existence of an extra force driving the mass loss will thus modify the shape of the equipotential surfaces, which are now defined as

$$\Phi = -\frac{\tilde{\mu}}{r_1} - \frac{(1-\tilde{\mu})(1-f)}{r_2} - \frac{x^2+y^2}{2} = \text{constant}, \tag{7}$$

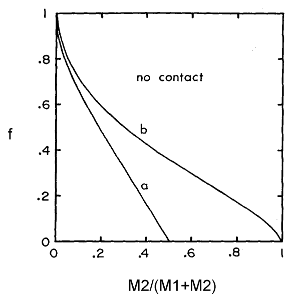

Fig. 3. The curve labeled b corresponds to $f = f_c(\tilde{\mu})$; i.e., the inner Lagrangian point and the external Lagrangian point opposite the mass-losing star share the same equipotential. Curve a corresponds to the situation where the two external Lagrangian points share the same equipotential (only possible when $1 - \tilde{\mu} < 0.5$). Systems with f lying above the curve labeled b (i.e., $f > f_c$) have no figure-eight equipotential surrounding the two stars. Systems to the left of curve a are topologically similar to the case $f = 0$ in the bottom panel of Figure 2. Systems between curves a and b are topologically similar to the case $f = 0$ in the upper panel of Figure 2. From [120].

where all symbols are the same as in (1) and it is assumed that star 2 is exerting radiation pressure on its wind. If f is assumed to be the same at all points, the equipotential surfaces may be easily derived from (7). Figure 2 shows that when f becomes larger than some critical value f_c (depending upon $\tilde{\mu}$, as given by curve b in Figure 3), there is no longer a critical Roche equipotential surrounding the two stars. In particular, when $f = f_c(\tilde{\mu})$, the critical Roche equipotential degenerates into a surface including *both* the inner Lagrangian point and the outer Lagrangian point opposite the mass-losing star, as shown in Figure 2 (to be compared with Figure 1). Matter flowing through L_1 will thus not necessarily be confined to the lobe surrounding the accreting component, but may escape from the system through the outer Lagrangian point, or may form a circumbinary disk. *This possibility is especially appealing in view of the frequent occurrence of such disks around post-AGB stars* (see **Chapter ??**). It should, however, be noted that for these modifications to the usual Roche geometry to become effective (they have been reported as well for X-ray binaries involving mass-losing supergiants [10, 62]), it is necessary that the wind remain optically thin; otherwise, it will be shielded from the irradiating star, and the extra force will disappear.

2.1.3 Radii of AGB Stars

The radius R of an AGB Mira star of mass M may be related to its pulsation period P using predictions from the pulsation theory fitted to linear diameters of Miras (as derived in [139] from angular size measurements and Hipparcos parallaxes):

$$\log R_{\rm Mira} = (\log P + 0.9 \log M + 2.07)/1.9 \text{ fundamental mode,}$$
$$\log R_{\rm Mira} = (\log P + 0.5 \log M + 1.40)/1.5 \text{ first overtone mode,} \tag{8}$$

where P is expressed in days, and R and M in solar units. The above relation also applies to those among the semiregular variables that fall along the same $P-L$ relation as the Mira variables. The question of whether Mira stars are pulsating in the fundamental or first overtone mode has been much debated (e.g., [149, 152, 153]), although recent evidence points to the fundamental mode (**Chapter ??**). The two possibilities will nevertheless be considered in the following discussion. Since AGB stars have very extended atmospheres, their radius is an ill-defined quantity. It is therefore necessary to specify that the above relations provide the so-called Rosseland radius (see [36] for a detailed discussion), which links the effective temperature to the bolometric luminosity. For non-Mira M stars, an empirical relationship between radii and spectral types has been derived [25], with radii ranging from a median value of 50 $R_\odot$ at M0III to 170 $R_\odot$ at M7/8III. These values are somewhat smaller than the Mira radii (250 $R_\odot$ for $P = 300$ d and $M = 1$ $M_\odot$ in the fundamental mode and 385 $R_\odot$ in the first overtone), as obtained from (8).

2.1.4 AGB Stars in Detached Binary Systems

To hold within a binary system, the radius R of the AGB star (supposed to be a Mira variable) derived from (8) must be smaller than the critical Roche radius R_R expressed by (2) (a brief discussion of the consequences of the situation $R > R_R$ will be presented in Section 4.4). The orbital period for which a Mira of a given pulsation period (in either the fundamental or first overtone mode) fills its Roche lobe is displayed in Figure 4. It is derived from the above formulae (7) and (8), and from Kepler's third law (assuming typical masses for the AGB star and its companion, as indicated on the figure). Note that the results presented in Figure 4 assume that there is no radiation pressure acting on a wind (i.e., $f = 0$ in (7)). Accounting for such a radiation pressure may severely alter the results, as further discussed in Section 2.1.2.

These orbital periods are quite long (more than 1000 d), and are always much longer than the pulsation periods. The corresponding radial-velocity semiamplitudes K (Figure 4) may be computed from the relation [123]

$$K = 212.8\ f(M_{\rm AGB}, M_{\rm comp})^{1/3}\ P^{1/3}\ (1-e^2)^{-1/2}, \tag{9}$$

where K is expressed in km s^{-1}, $f(M_{\rm AGB}, M_{\rm comp}) = M^3_{\rm comp} \sin^3 i/(M_{\rm AGB} + M_{\rm comp})^2$ is the mass function expressed in $M_\odot$, e is the orbital eccentricity, i the orbital inclination, and P the orbital period expressed in days. This quantity will prove to be important for comparison with the intrinsic radial-velocity variations of AGB stars (due to pulsations) to be discussed in Section 2.2.1.

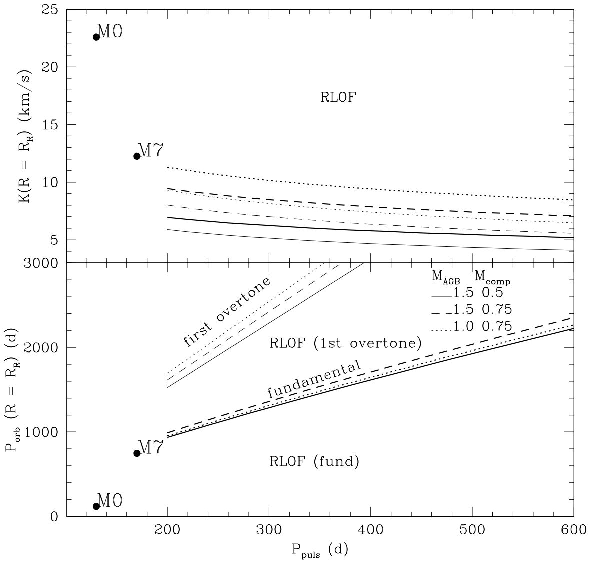

Fig. 4. Bottom panel: Orbital periods versus pulsation periods for Miras in semidetached systems, derived from the period–radius relations (8) for the fundamental and first overtone modes. Detached systems are located above the corresponding lines. The filled circles labeled M0 and M7 indicate the critical periods corresponding to the median radii of non-Mira M0 and M7 giants, respectively (adopting masses of 1.0 and 0.75 $M_\odot$ for the giant and its companion, respectively). **Top panel**: Orbital radial-velocity semiamplitude versus pulsation periods (thick line: fundamental mode; thin line: first overtone) for Miras in circular semidetached systems with $\sin i = 1$ (where i is the orbital inclination). Binary systems with larger semiamplitudes would involve Roche-lobe-filling AGB stars.

2.2 Binary Systems Involving AGB Stars

Before discussing the methods available to identify binary systems involving AGB stars, it is necessary to define first observational criteria that may be used to identify an AGB star. The following three criteria have been used in this section: The star exhibits spectral lines from the unstable element technetium (Section 4.1.1), or is of spectral type C (although this may not be a sufficient condition given the intrinsic/extrinsic paradigm discussed in Section 4.1.2), or is a Mira variable. It must not be excluded, however, that some AGB stars might not bear these distinctive properties. Such “dormant” AGB stars, indistinguishable from RGB stars of similar luminosity or from massive supergiant stars, are thus missing from the statistics of binary AGB stars presented in this section. This remark applies especially to the class of VV Cep and ζ Aur binaries (late-type supergiants that are either genuine massive stars, or very luminous AGB stars, with an A-BV companion eclipsed by the extended atmosphere of the supergiant [14]), and to the many binary (often, but not always, symbiotic) systems involving a non-Mira M giant (RGB or AGB star? see especially [40] for a list of binary systems involving semiregular variable stars).

The methods available to find binary systems involving AGB stars are the following:

- Radial-velocity variations
- Presence of a visual companion
- Composite nature of the spectrum and/or symbiotic activity
- X-ray emission
- Shallow light curve of a Mira variable, with wide and flat minima
- Light variations associated with orbital motion (eclipses, Algol)
- Lunar occultations
- Imaging of CSE asymmetries

Binaries discovered by these methods, which are commented in the remainder of this section, are listed in Table 1. This table is, to the author's best knowledge, supposed to list all binaries involving an AGB star known as of mid-2001.

2.2.1 Radial-Velocity Variations: Intrinsic Versus Orbital

No convincing case of a spectroscopic binary involving an AGB star (defined according to the "working" criteria given at the beginning of Section 2.2) is currently known,[3] basically because orbital radial-velocity variations are confused by the intrinsic variations associated with the envelope pulsation (Figure 5; see also [40]). However, since spectroscopic orbits give (partial) access to the stellar masses, radial-velocity surveys are worth pursuing despite the confusion introduced by the pulsation. With a good understanding of these intrinsic radial-velocity variations, it may be hoped that orbital and intrinsic variations may in the end be disentangled [4, 40].

The semiamplitude of the radial-velocity variations associated with the pulsations of Mira and semiregular variable stars is displayed in Figure 6. For both the Mira and the semiregular variables, there is a good correlation between the radial-velocity semiamplitude and the visual amplitude. In contrast, Miras exhibit little correlation between their periods and radial-velocity semiamplitudes, which lie in the range 10–15 km s^{-1}. Semiregular variables have radial-velocity semiamplitudes increasing with the period, from a few km s^{-1} up to the values typical of Miras.

The above considerations thus allow one to draw a fairly accurate picture of the intrinsic variations exhibited by Mira stars, an essential prerequisite to search for binaries among AGB stars. From the comparison of Figures 4 and

[3] The fact that all Tc-poor S stars are spectroscopic binaries (Table 7) does not contradict this statement, since these stars are not AGB stars.

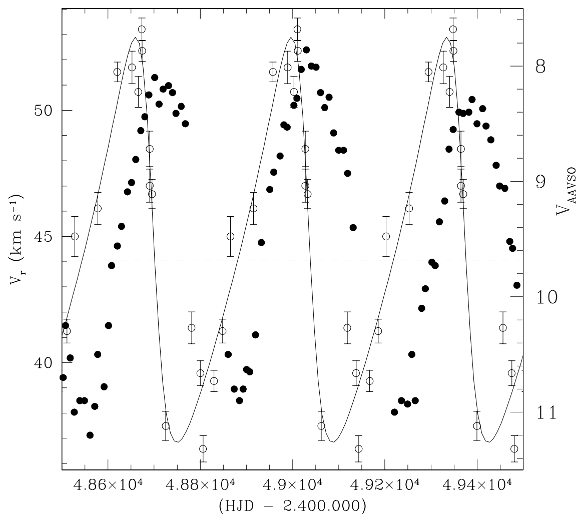

Fig. 5. AAVSO light curve (filled dots) for the CS Mira variable R CMi during three successive cycles, compared to its radial-velocity curve (solid line and open dots, from [135]). Radial-velocity measurements were not necessarily obtained at the indicated dates, as they were all folded onto the radial-velocity solution

6, it appears that the properties of the Mira intrinsic radial-velocity variations locate them in the forbidden (labeled RLOF in the upper panel of Figure 4) region of the period–semiamplitude diagram of *binary* systems. There is therefore in principle no overlap between the parameter ranges characterizing orbital and intrinsic radial-velocity variations of Miras. This property may in fact be of some help in correctly identifying the nature of the observed radial-velocity variations. Nevertheless, orbital variations remain difficult to detect, since for the reasonable choice of masses displayed in Figure 4, orbital variations of Miras in detached binary systems are smaller than the semiamplitudes of the *intrinsic* radial-velocity variations (Figure 6). *It is therefore clear that the detection of binary systems involving Mira stars with radial-velocity techniques is a difficult operation, because (i) the time scales involved are quite long (several years) and (ii) the orbital radial-velocity variations are smaller than the intrinsic variations. Binary systems will therefore basically show up as a long-term trend superimposed on intrinsic variations characterized by a shorter time scale.*

Radial-velocity monitoring surveys of AGB stars have been scarce so far. A monitoring of 9 multiperiodic semiregular variable stars has yielded one possible binary [40] (AF Cyg, not listed in Table 1 because semiregular variables do not fulfill the strict AGB criteria outlined at the beginning of Section 2.2).

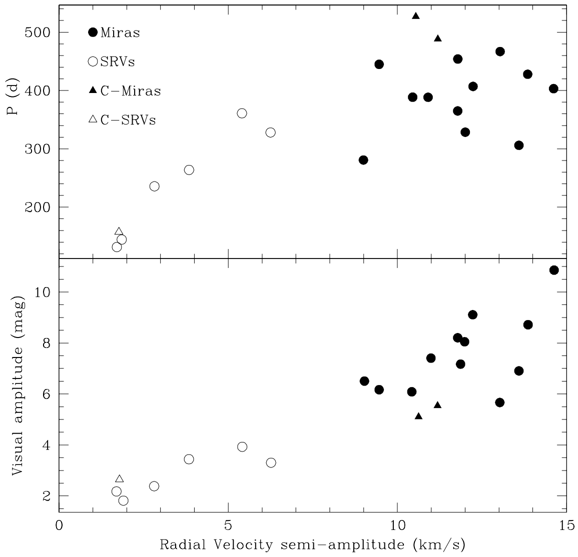

Fig. 6. Top panel: Correlation between the radial-velocity semiamplitude (as derived from the 1.5–2.5 μm CO lines) and the period of the visual lightcurve for stars from various classes of long-period variables.
Bottom panel: Same as top panel for the visual amplitude. Adapted from Figure 10 of [41].

Among the 81 long-period variables monitored in [4], binarity could be efficiently checked in 9 stars only, with one possible binary candidate emerging (S Cam). Among the 13 Mira S stars, 7 SC/CS stars, and 3 C stars monitored in [135], only one (S UMa) has revealed a possible signature of binary motion, but this signal might well in the end turn out to be a 1-y alias of the Mira pulsation period.

2.2.2 Visual Binaries

A list of Mira and semiregular variables in visual binary systems is provided in [109]. Only those systems with a separation smaller than 5″ have been listed in Table 1. The *Third Catalogue of Interferometric Measurements of Binary Stars*[4] has been scanned for Mira variables and carbon stars. Among the 38 carbon and Mira stars with interferometric measurements found in the database, only X Oph is a firm detection, all the other cases being either ambiguous detections or nondetections. Several carbon stars are listed as double

[4] Hartkopf et al., CHARA Contribution No. 4, 1999, available at `http://www.chara.gsu.edu/DoubleStars/Speckle/intro.html`

stars by the *Hipparcos Catalogue*, but subsequent speckle observations did not confirm their binary nature [76, 105]. Speckle observations of 33 semiregular and Mira variables aimed at detecting binary stars among late-type stars resulted in three positive detections, all listed in Table 1 [108].

The orbits available for X Oph and Mira Ceti [108] yield system masses of 20.9 and 4.4 $M_\odot$, respectively. Such a large value for X Oph appears very unlikely, and simply reflects the poor quality of the available parallax and of the orbital elements for such a long-period system. The situation appears somewhat better for Mira Ceti. Adopting a WD mass of 0.6 $M_\odot$, this preliminary orbit thus yields a mass of about 3.8 $M_\odot$ for Mira itself, but since its orbit is not yet fully constrained by the available observations, this mass still bears considerable uncertainties.

2.2.3 Composite Spectrum and Symbiotic Activity

The composite (or "symbiotic") nature of the spectrum has delivered several binary systems involving AGB stars (Table 1). At this point, it should be mentioned that the low discovery rate of binaries among non-symbiotic AGB stars may simply result from the fact that AGB stars in binary systems necessarily develop a strong symbiotic activity triggered by the interaction of their strong wind with their companion, as will be discussed below. Hence, most, if not all, binaries involving AGB stars may in fact appear as symbiotic stars. In this respect, it is interesting to note that the *Eighth Catalogue of the Orbital Elements of Spectroscopic Binary Stars* [8] contains 20 systems with M giant or supergiant primaries, among which 14 are in fact symbiotic systems. Moreover, it is worth noting that Mira Ceti itself is member of a binary system, which, despite its large orbital separation (Table 1), nevertheless exhibits some symbiotic activity [112]. Symbiotic stars are defined[5] as having peculiar spectra merging low-excitation absorption features (TiO bands, neutral metal lines) with high-excitation emission lines (like He II λ4686; Figure 7). Nebular features like forbidden lines[6] requiring low densities, are frequently present as well. Moreover, far-UV spectroscopy reveals the presence of a hot blackbody continuum (characterized by temperatures sometimes in excess of 10^5 K and luminosities in the range 10–1000 $L_\odot$) that makes it clear that symbiotic stars are in fact binary systems involving a cool giant and a hot compact star (either on the main sequence or, more generally, a WD) accreting matter from its companion. The hot continuum is emitted by the compact companion, which is heated by the accretion of the wind from the red giant star.

[5] See *Symbiotic stars probing stellar evolution* (edited by R. Corradi & J. Mikołajewska, Astron. Soc. Pacific Conf. Ser., 2003) for the latest developments on symbiotic stars.

[6] Forbidden lines correspond to radiative transitions not allowed by the first-order quantum-mechanical selection rules. These lines are not observed in high-density environments, where the collisional deexcitation of the upper level is much faster than its radiative deexcitation.

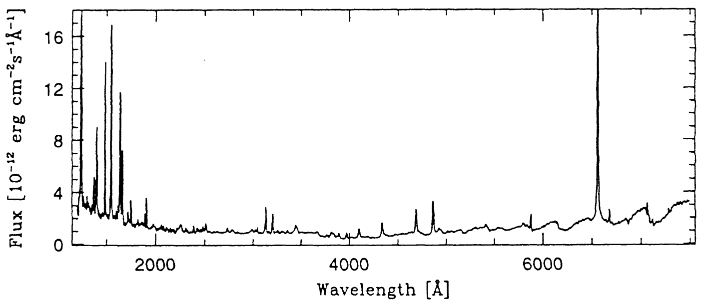

Fig. 7. Optical/ultraviolet spectrum of the symbiotic star AG Peg showing the hot UV continuum, the emission lines, the Balmer continuum in emission, the cool-star continuum and its absorption bands. From [92].

Symbiotic activity involves **eruptions** either caused by thermonuclear flashes at the surface of white dwarfs accreting at a slow rate ($< 10^{-9}$ $M_\odot$ yr^{-1}, as in the case AG Peg), or by instabilities in the accretion disk (for main-sequence stars accreting from a Roche lobe-filling giant like CI Cyg), **dust obscuration episodes** (in symbiotic Miras like R Aqr or BI Cru; see Section 3.2) and **reflection effect** caused by the heating of the cool component atmosphere facing the hot component.

Symbiotic stars form a heterogeneous family (see [9] for the most recent catalogue, comprising 188 symbiotic stars). A first classification involves the spectrum of the cool component: *Yellow* symbiotics comprise G or K giants, whereas *red* symbiotics comprise M giants. A second classification refers to their IR properties: *d-type* symbiotics ("dusty") have IR excesses indicating the presence of circumstellar dust and generally host a Mira variable (*d'-type* applies to dusty *yellow* symbiotics), whereas *s-type* ("stellar") symbiotics (not to be confused with stars of spectral type S) have infrared colors consistent with their photospheric temperature. Symbiotic Miras with an entry in the *General Catalogue of Variable Stars* (GCVS) are BI Cru (280 d), KM Vel (370 d), RX Pup (580 d), V704 Cen (?), HM Sge (540 d), V1016 Cyg (450 d), RR Tel (387 d), and R Aqr (387 d). The sample of symbiotic Miras has an average period of 424 d (with a range extending from 280 to 580 d), which is larger than the average for field Miras from the GCVS [147]. The reason why symbiotic stars tend to host long-period Miras is currently unclear (selection effect against long-period, obscured Miras in the GCVS, or rather stronger mass loss associated with long-period, high-luminosity Miras necessary to trigger the symbiotic activity?).

2.2.4 X-ray Emission

X-rays are normally not observed in single M giants lying to the right of the so-called dividing line, an almost vertical boundary in the HR diagram separating stars with hot coronae emitting X-rays (to the left) from stars with high mass loss (to the right) [44]. In a binary system, several processes may generate X-rays. First, X-rays may be produced at the shocks resulting from the collision of streams in the complex flow pattern associated with wind accretion in a detached binary system involving an AGB star (Section 3.1). Second, X-rays are generated when the gravitational energy of the AGB wind falling in the potential well of the companion star (of mass $M_{\rm comp}$ and radius $R_{\rm comp}$) is converted into radiative energy when impacting the stellar surface. The accretion luminosity

$$L = G\ \dot{M}_{\rm acc}\ M_{\rm comp}/R_{\rm comp}, \tag{10}$$

where G is the gravitational constant and $\dot{M}_{\rm acc}$ is the accretion rate, will either be radiated away in the form of hard X-rays if the infalling matter is optically thin, or if that matter is optically thick, half will be converted into thermal energy and half will be radiated away in the form of blackbody radiation (according to the virial theorem).

A search for X (or far-UV) sources among AGB stars is therefore an efficient way of finding binary systems involving AGB stars. In fact, this method is a corollary of the search for symbiotic activity, since symbiotics are generally strong X-ray emitters. The ROSAT all-sky survey of X-ray sources detected only 11 out of 482 M giants of luminosity classes I to III from the *Bright Star Catalogue* [44]. Of those 11 sources, one is the well-known symbiotic star R Aqr; another is 4 Dra, a triple system with a cataclysmic binary as a secondary; two have close G-type secondaries (η Gem and α Her), which are the likely sources for the observed coronal X-ray emission; and 3 sources probably result from spurious associations. None among the 4 stars remaining as candidate symbiotic systems exhibits the typical emission lines expected in the optical.

2.2.5 Light Curves

Light curves of long-period variables that are either shallow or have wide, flat minima may be indicative of the presence of a companion dominating the system light at minimum [91, 141]. These expectations are not borne out by spectroscopic inspection [38], which revealed composite spectra for only a few among these candidates. Among 23 shallow light curves for S stars, only W Aql, WY Cas, and T Sgr turn out to have a composite spectrum. Among the 55 candidate M stars, only R Aqr and possibly RU Her have composite spectra. Visual companions have also been found for Z Tau and X Oph.

The analysis of the MACHO light curves [152] raised the intriguing possibility that 25% of all AGB stars in the LMC might be semidetached binaries (see **Chapter ??**), but recent observations have challenged this claim [40].

2.2.6 Lunar Occultations

The binary nature of AGB stars may also be revealed by lunar-occultation observations, provided that the magnitude difference between the AGB star and its companion be not too large (< 3.5 mag [113]). Four candidate binary AGB stars have been reported so far [114].

2.2.7 Imaging of Asymmetries in CSEs

The copious amount of mass lost by AGB stars through winds feeds their CSEs. Despite the fact that all CSEs deviate to some extent from homogeneity and spherical symmetry (**Chapter ??**), stronger and very typical deviations may be expected in binary systems. Their detection by direct imaging may serve as an indicator of the binary nature of the underlying star. Specific and readily identifiable flow patterns may be expected in a binary system, as discussed in Section 3.1. Table 2 lists those stars where the CSE has been imaged and reveals complex structures most probably due to the binary nature of the underlying star.

A related diagnostic involves the detection of a circumbinary disk (Section 3.1) through the associated very narrow (FWHM $< 5\,\mathrm{km\ s^{-1}}$) CO radio line emission [55]. The detection of such features around the J-type carbon stars EU And and BM Gem [55] thus leads to the intriguing suggestion that the class of J stars might contain a large proportion of binary stars (further evidence in this respect is presented in Section 4.2.1).

3 Impact of Binarity on Intrinsic Properties of AGB Stars

3.1 Mass-Loss Geometry

The presence of a companion to the AGB star is expected to alter the geometry of the wind blowing off the AGB star. The geometry of mass flows in detached systems involving an AGB star is governed by the fact that the wind velocity v_∞ (typically 15 km s^{-1}; **Chapters ?? and ??**) is of the same order of magnitude as the relative orbital velocity $v_{\rm orb}$ [on the order of $K_{\rm AGB} + K_{\rm comp} = K_{\rm AGB}(1 + M_{\rm AGB}/M_{\rm comp})$, where K is the semiamplitude of the velocity variations as given by Figure 4 for the AGB star]. Coriolis effects are therefore important, and lead to intricate flow patterns. In the classical description of the flow past a compact object [13], the flow is assumed to be plane-parallel at infinity and without any transverse density or velocity gradients (this situation holds, for example, in X-ray binaries involving fast winds from hot stars, where $v_\infty \gg v_{\rm orb}$). The gravitational field of the compact star bends the flow and makes the streams passing on each side of the compact star collide with each other. This collision results in the formation of an accretion

Table 1. A list of AGB stars (identified by their Tc-rich, C-rich or Mira nature) in binary systems. In column Var., M stands for Mira, SR for semiregular. The column Sep. provides either the angular semimajor axis of the relative orbit (X Oph only) or the angular separation on the sky. The column Comp. provides the spectral type of the companion when known (WD stands for white dwarf). Among symbiotic systems, only carbon symbiotics and Mira symbiotics with an estimated $P_{\rm orb}$ are listed (see [9] for an exhaustive catalogue).

Name	Sp.	Tc	Var.	$P_{\rm phot}$ [d]	$P_{\rm orb}$ [d]	Sep. [″]	Comp.
Composite spectra							
HD 172481	MIII	?	M	312			F2Ia (p-AGB)
RU Her	M6e-M9	y?	M	485			? [a]
IRC −20197 [e]	M9	?	M	636		≈1	A-FV
W Aql	S6/6e	?	M	490			F5-8V
WY Cas	S6/6e	?	M	476			GV
T Sgr	S5/6e	y	M	394			F3IV
SZ Sgr	C7,3	y?	SRb	100:		1.9	A7V
TU Tau	C5,4	?	SR:	190			A2V:
DM−26°2983	C4,4	?	?	?			A5V
Symbiotic carbon stars							
UV Aur	C8,1Je	y	SRb	393.4		3.4	
SS 38	C9	?	M?	?			
AS 210	C	?	M?	?			
HD 59643	C6,2	?	SR?	70			
V335 Vul	Ce	?	SR	?			
Symbiotic Mira stars with estimated $P_{\rm orb}$ [d]							
Mira Ceti	M7IIIe	y	M	331.6	$>3.6\times10^4$	0.6	Be/WD [b]
R Aqr	M7	y?	M	387	1.6×10^4?	0.055	?
V1016 Cyg	> M4	?	M	450	3×10^4?		?
Visual binaries							
HDE 308122	M6-8e	?	M	320		4	K0III
(= CpD -62° 1837)							
RV Cam	M4II-III	?	SRb	101		0.07	
RY Cam	M3III	?	SRb	136		0.06	
RU Cap	M9e	?	M	346.9		1.6	
R Car	M4-8e	?	M	308.7		2	
T Dor	M5IIe	?	M	168		4.8	
π^1 Gru	S5,7	y	SRb	150		2.7	G0V
U Men	M3	?	SRa	407		0.6	K0III-IV
X Oph	M5/9IIIe	y?	M	334	1.8×10^5	0.34	K1III
SV Peg	M7	?	SRb	145		0.44	
SU Sgr	M7III	?	SRb	88		1.1	
Z Tau	S7.5,1e:	?	M	494		4	
Lunar occultations							
EI Tau	S	?	SRa	364		0.007	
V1203 Oph		?	M			0.050	
CGCS 3964	C	?				0.020	
ZZ Gem [c]	Ne	?	M	317		0.088	

[a] The composite spectrum is doubtful.
[b] The Be spectrum of the companion actually corresponds to an accreting WD.
[c] Binary nature not confirmed by speckle observations (see [75]).
[d] see [147] for a complete list.
[e] Also an OH maser.

Table 2. A list of AGB stars with a nonspherical CSE shaped by the binary nature of the underlying star. The various shapes encountered are discussed in Section 3.1.

Name	Type	Shape	λ [μm]	Ref.
π^1 Gru	S(Tc) SRb	disk + fast polar jets	CO(J=2-1)	[61, 117]
V Hya	carbon Mira	fast bipolar wind, eclipses by CSE dust orbiting a comp. (17-yr period)	CO(J=2-1)	[60]
o Ceti	Mira	hook towards comp.	0.346	[57]
		quadrupolar struct.	1.65	[22]
		clump around comp.	11	[71]
EU And BM Gem	J(no-Tc)	circumbinary disk	CO(J=2-1)	[2, 55]
HD 44179 (="Red rectangle")	post-AGB	circumbinary disk	0.656	[100]
Various symbiotics		bipolar and/or spiral jet	0.658	[17]
M 2-9	PN hot WD+AGB	bipolar nebula, fast jet rotating with a $\approx$120 yr period	0.55	[69]

column (tilted by an angle $\alpha = \arctan v_{\rm orb}/v_\infty$ with respect to the line joining the two stars), with matter falling onto the compact star from its rear side (as viewed from the mass-losing star) at a rate [130]

$$\dot{M}_{\rm acc,B\text{-}H} = -\alpha\mu^2 \frac{k^4}{[1+k^2+(c/v_\infty)^2]^{3/2}} \dot{M}_{\rm AGB}, \tag{11}$$

where the subscript B-H stands for "Bondi–Hoyle," α is a parameter of order unity, $\mu \equiv M_{\rm comp}/(M_{\rm comp}+M_{\rm AGB})$, $k \equiv v_{\rm orb}/v_\infty$, $c_{\rm s}$ is the sound velocity, and $\dot{M}_{\rm AGB}$ is the wind mass-loss rate of the companion AGB star. No accretion disk is predicted from accretion in the Bondi–Hoyle regime, since the colliding flows are perfectly symmetric and there is thus no accretion of spin momentum either.

The situation relevant to detached binary systems involving an AGB star and characterized by $v_\infty \approx v_{\rm orb}$ is much more complicated than the Bondi–Hoyle regime, and must be investigated numerically. Figure 8 presents the flow structure from one of the very few 3D hydrodynamical simulations currently available [27, 78, 130].

The parameter space is quite vast (orbital separation, component masses, mass loss rate, AGB star co-rotating with the orbit or not, ratio wind/orbital

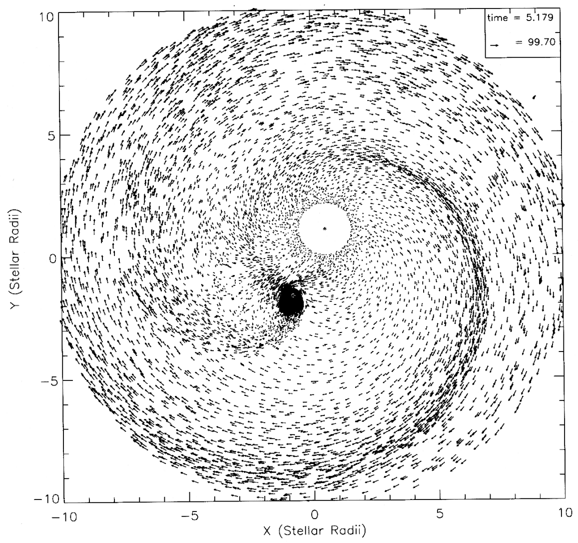

Fig. 8. Velocity field of the wind and accretion wake in the orbital plane, in a corotating frame (i.e., where the stars are at rest). The orbital period is 4.5 yr, $M_{\rm AGB} = 1.5\,{\rm M}_\odot$, $M_{\rm comp} = 1\ {\rm M}_\odot$, $v_\infty = 9\,{\rm km\ s}^{-1}$. The AGB star is in synchronous rotation with the orbit, and its radius is one-third of the orbital separation (or 0.8 R_R). From Figure 12b of [77].

velocities, presence of a wind blowing off the companion, etc.), and remains largely unexplored. General flow features emerging from the explored cases are as follows (Figure 8):

(i) Funneling Through L1

Even in detached binary systems, the wind from the mass-losing star is funneled through the inner Lagrangian point L_1 (Figures 1 and 8). This funneling results from the very geometry of the Roche potentials, and causes a substantial density enhancement and heating of the gas stream around L_1.[7] It is visible in Figure 8 as a curved stream between the two stars. Such a gas stream has been detected [122] in the 596 d detached binary HR 1105 (Tc-poor S star + WD) through the orbital modulation of the profile and intensity of the high-excitation line He I λ1083 nm. This stream may also perhaps correspond to the hook-like appendage to Mira Ceti A observed in the UV [57] and pointing toward Mira B (Table 2).

(ii) Accretion Disk

The flow funneled through L_1 is curved by the Coriolis force, which introduces

[7] The wind leaving the AGB star from the hemisphere facing its companion is expected to be denser [28], and this effect, not taken into account in the simulation displayed in Figure 8, would even reinforce the density enhancement around L_1.

the asymmetry responsible for the formation of an accretion disk around the companion. This result contrasts with the prediction that no accretion disk forms in the Bondi–Hoyle wind-accretion regime. The formation of a disk has been observed in all the 3D numerical simulations currently available [78, 130]. It is stable (no flip-flop instability as observed in 2D simulations), thin, and tilted with respect to the orbital plane, and thus probably precessing. A precessing disk coupled with intermittent polar jets (although those are not obtained in the above simulations) might play a role in the formation of bipolar or even quadrupolar structures observed in several symbiotic, Mira and post-AGB binary stars (see Section 2.2.7). The prediction of an accretion disk forming during wind accretion is important, because it offers the possibility of accounting for the very commonly observed bipolar structures without invoking the much more transient and dramatic RLOF for producing the required disk, as in [93]. Observational evidence for accretion disks in detached binary systems has been found for o Ceti, 56 Peg (K0IIBa + WD), and HD 35155 (Tc-poor S + WD, $P = 640.5$ d).

(iii) Spiral Arm

The flow pattern of Figure 8 exhibits a very clear double spiral arm, a feature obtained in all the other 3D-simulations of wind accretion in detached binary systems. They may be seen as forming the boundaries of the accretion wake, strongly curved by the action of the Coriolis force. These spiral arms correspond to the shocks caused by the collision of the wind coming directly from the AGB star with the accretion wake.

(iv) Circumbinary Disk

The formation of a circumbinary disk seems common in binary systems with a mass-losing star (especially those involving post-AGB stars; see **Chapter ??**), as revealed by direct imaging, the clearest example being the "Red Rectangle" (HD 44179) [100]. Further, albeit indirect, support for the presence of circumbinary disks is provided by the orbital modulation observed in the light curve of several post-AGB systems (see **Chapter ??**), which is best interpreted by variable obscuration from dust trapped in such a disk. Finally, the very narrow CO circumstellar lines (FWHM < 5 km s^{-1}) exhibited by several post-AGB systems [55] also point to gas orbiting the system in a circumbinary disk, rather than flowing out with velocities of order 10–20 km s^{-1}, typical of AGB winds (**Chapters ?? and ??**).

A circumbinary disk does not, though, clearly emerge from the currently available 3D simulations of wind accretion in detached binaries. It is possible, however, that the extended spiral arm, winding around the system, mimicks a circumbinary disk (Figure 8). Alternatively, a circumbinary disk may form during RLOF if matter is expelled not only through L_1 but also through L_3 (Figure 1), as discussed in Section 2.1.2.

3.2 Mass Loss and Dust Formation

The flow pattern described in Section 3.1 includes several regions where the wind is compressed. These regions of high density will favor dust formation, provided that the corresponding temperature does not exceed the dust condensation temperature (about 1500 K, depending on its chemical composition; **Chapter ??**). Empirical evidence seems indeed to support the idea that dust formation may be easier in binary systems. First, dust obscuration episodes are frequent in symbiotic Miras and much rarer in single M-type Miras [94, 147, 148]. Similar behavior is observed in the K0III Ba3 + WD system HD 46407 (P = 457 d) [50]. This system involves a K giant with a low mass-loss rate where dust formation is not at all expected. Nevertheless, dust-obscuration episodes seem to be the best explanation for the observed light variations. Finally, dust seems to form in the wind of binary WC stars [21]. Although the latter two systems do not involve AGB stars, they serve to illustrate that dust may form in binary systems, despite rather hostile environments.

The dust formed in a binary system may be stored in the long-lived circumbinary disks observed in many instances, especially in systems involving post-AGB stars and silicate J-type carbon stars (Section 3.1 and **Chapter ??**).

3.3 Mass-Loss Rate

The possibility that stars in binary systems lose mass at a faster rate than their nonbinary counterparts must be considered seriously, since the presence of the companion will reduce the effective gravity of the mass-losing star, thus enhancing the mass loss [28].

This enhancement has been considered necessary to stabilize RLOF in those binary evolution channels leading to observed systems like Algols and short-period barium stars that would otherwise end up as cataclysmic variables (see Section 4.4). The key argument here is that the *companion-reinforced attrition process* (CRAP) [134] will reverse the mass ratio before the onset of RLOF, thus making it dynamically stable (see the discussion after (25)). As will be discussed in Section 4.4, CRAP is not, however, the only way to account for the short-period barium systems (see the discussion in relation to Figure 11). Besides these indirect theoretical arguments, the very large CO mass-loss rates observed for the binary AGB stars W Aql, WY Cas, and S Lyr [52] may provide some support to CRAP, although binary AGB stars like T Sgr and π^1 Gru have mass-loss rates close to the average for stars of their kind. Since orbital separations are not available for these systems, it is difficult to draw conclusive statements on the impact of binarity on the mass-loss rate. Nonetheless, detailed theoretical considerations indicate that mass loss from red giants in binary systems is enhanced by a factor $(R/R_R)^3$, where R is the radius of the mass-losing giant [28].

3.4 Masers

The maser activity of AGB stars and their binarity seem to be quite clearly anticorrelated. Direct evidence thereof is provided by the almost total lack of SiO masers among symbiotic stars containing a Mira variable [121], with the exception of the very wide binary R Aqr (Table 1). On the other hand, very wide systems like o Ceti, R Aqr, and X Oph (Table 1) lack the OH maser, which involves layers several 10^5 $R_\odot$ away from the star, in contrast to the SiO maser, which forms close to the photosphere (**Chapter ??**). A survey of IRAS sources [63] reveals that the region occupied by OH/IR sources in the IRAS color–color diagram also contains many stars with no OH masing activity. Furthermore, detected and undetected OH maser sources have identical galactic latitude distributions. These two facts find a natural explanation if binarity is the distinctive property between detections and nondetections. The role of binarity in preventing the maser activity was already suspected on theoretical grounds [39], since the presence of a companion periodically disturbs the layer where maser activity should develop. There should actually be a critical orbital separation for every kind of maser below which the companion sweeps through the corresponding masing layer [121], thus preventing its development ($A < 10\,\mathrm{AU}$: no masing activity; $10 \le A(\mathrm{AU}) < 50$: SiO and H_2O masers possible but no OH maser; $A > 50\,\mathrm{AU}$: all masers can operate).

3.5 Coupling Between Pulsation and Orbital Motion

In systems that are close enough for tides to develop on the AGB star, the possibility exists for a resonance between the dynamic tide and a free oscillation mode, as suggested in the seminal paper [20]. This possibility has been investigated theoretically for close binaries involving upper main sequence stars (e.g., [151]), but not, to our knowledge, for AGB stars in binary systems. A possible coupling between the orbital motion and a (probably nonradial) pulsation has been reported for the symbiotic star AG Dra [29].

3.6 Abundances

The impact of binarity on abundances is clearly established for those post-AGB stars that are very metal-deficient, as a result of a fractionation process occurring in relation with the circumbinary disk (see **Chapter ??** for a more detailed discussion). Another obvious link between abundances and binarity is the accretion by the companion of the AGB wind enriched in carbon and heavy elements. This mass-transfer process accounts for the zoo of chemically peculiar late-type stars (see Section 4).

Carbon stars belonging to the R and J types may also somehow bear their peculiar abundances from binarity, although the chain of events linking the two properties has not yet been uncovered. Binary-induced mixing rather than mass transfer may be at play here (Section 4.2.1).

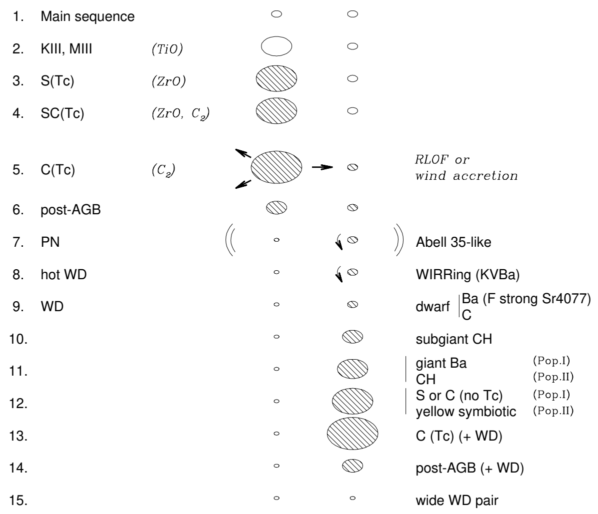

Fig. 9. The evolution of a system consisting initially of two low- or intermediate-mass main-sequence stars. The left column corresponds to the normal evolutionary sequence of single stars, while the right column represents the various classes of stars with chemical peculiarities specifically produced by mass transfer across the binary system. Hatched circles denote stars with atmospheres enriched in carbon or heavy elements.

4 The progeny of AGB stars in binary systems

Section 2 dealt with systems where the primary star is currently an AGB star. At this stage, the mass lost by the AGB star interacts with its companion and imprints several observable signatures (fast rotation, chemical anomalies, etc.). The remainder of this chapter is devoted to the description of the rich progeny of AGB stars in binaries, namely, binary systems with a WD component (i.e., the end product of the former AGB star) and a primary star polluted by the mass transferred from the former AGB star.

The evolution followed by a system consisting initially of two low- or intermediate-mass main-sequence stars is sketched in Figure 9. The systems where the primary star is an AGB star (according to the "working" definition given at the beginning of Section 2.2) correspond to cases 3 to 5 as well as 13 in Figure 9 (Note that cases 3–5 and 13 differ only in the nature of the companion: a main sequence star in the former case and a WD in the latter case). The present section deals with the evolution after the mass-transfer episode occurring at phase 5. That evolution will, in fact, depend on the mass-transfer mode itself (either wind accretion or RLOF), as discussed in

Section 4.4. The mass-transfer scenario was originally invoked to account for the chemical anomalies exhibited by barium stars (corresponding to phase 11 in Figure 9). These stars are G and K giants of too low a luminosity to be on the AGB, and whose overabundances of s-process elements can thus not be accounted for by internal nucleosynthesis (see also Section 4.2). Their origin remained a mystery until it was suggested [82] that the envelopes of barium stars may have been polluted by matter accreted from a former AGB companion (being now a dim WD [6]). Another important asset of the mass-transfer scenario is its ability to account for Tc-poor S stars. The observation in the spectra of *some* S stars, of lines from technetium, an element with no stable isotopes (Section 4.1.1), is a clear indication that these stars are TP-AGB stars where the s-process of nucleosynthesis is operating. It was unclear, however, why not all S stars exhibited Tc lines, until the mass-transfer scenario led to the formulation of the extrinsic/intrinsic paradigm; namely, two different kinds of S stars should exist: (i) *intrinsic*, genuine TP-AGB S stars with Tc lines (phase 4 in Figure 9), and (ii) *extrinsic*, Tc-poor S stars whose chemical anomalies result from a mass-transfer episode as for barium stars (phase 12 in Figure 9). Since the time elapsed between phases 4 and 12 is in general much longer than the Tc half-life, Tc has ample time to decay, and is therefore absent in extrinsic, binary S stars belonging to phase 12. The extrinsic/intrinsic paradigm of S stars will be discussed in more detail in Section 4.1.2. In fact, the mass-transfer scenario makes several predictions that are open to verification, namely, (i) the Tc-rich/Tc-poor dichotomy of S stars (phases 4 and 12 in Figure 9); (ii) all barium stars and Tc-poor S stars should be binaries; (iii) the existence of many other kinds of extrinsic stars (as listed in the right column of Figure 9, from phases 7 to 12); (iv) the companion of extrinsic stars should always be WDs; (v) the possibility of transiently forming rapidly rotating stars from the accretion not only of mass but also of spin angular momentum (phases 7 and 8); (vi) the evolutionary link between dwarf Ba or C stars, giant barium stars, and Tc-poor S stars (which should thus have similar orbital elements). All these predictions will be confronted with the observations in the following sections.

4.1 Technetium and the Extrinsic/Intrinsic Paradigm of S Stars

4.1.1 Tc in Stars

Among elements lighter than bismuth, technetium (Tc, atomic number 43) is (along with promethium; Pm, atomic number 61) the only chemical element with no stable isotopes. Technetium (after the Greek word $\tau\epsilon\chi\nu\iota\kappa o$ meaning "artificial") was discovered in 1937 by Segré and Perrier in a piece of molybdenium that had been irradiated with deuterons. It is also a fission product of uranium. Its longest-lived isotope (^{98}Tc) has a half-life of 4.2×10^6 yr. The isotope ^{99}Tc (laboratory half-life of 2.1×10^5 yr) is the only one produced by the s-process (see **Chapter ??**). Lines of Tc have been found in the S star

R And [89, 90] (see **Chapters ?? and ??** for a description of the principal spectral features of S stars), thereby giving strong support to the operation of the s-process followed by dredge-ups in thermally pulsing AGB stars.[8] In fact, *the presence of Tc in a star may be considered as the most reliable signature of its AGB nature.* A comparison of modern high-resolution spectra of Tc-rich S stars and Tc-poor S and M stars is presented in Figure 10. High-resolution spectra ($\lambda/\Delta\lambda \geq 30\,000$) are required to detect the Tc I lines, since the strong resonance lines of Tc I lie in the violet, where blending is very severe in the spectrum of cool stars. For example, the Tc I λ426.227 nm line is blended especially with Nd II λ426.223 and to a lesser extent with Gd II λ426.209 and Cr I λ426.237 (Figure 10). Very cool stars and carbon stars emit very little flux in that spectral region, so that the use of the weaker intercombination line at λ592.447 nm may be preferable.[9] In warmer stars ($T > 4000$ K), Tc is predominantly in the form Tc II, whose strong lines lie in the far UV at 264.70, 261.00, and 254.32 nm, accessible only through satellite observations. These UV lines have been used to look for Tc in barium stars and in the main-sequence A stars Sirius (α CMa A) and Vega (α Lyr), with negative results. This negative result bears some significance for barium stars and for Sirius, which exhibit heavy-element overabundances like S stars and are binaries with WD companions (Section 4.2). This result is precisely what is expected in the framework of the binary scenario sketched in Figure 9.

Since the pioneering work of Merrill, surveys searching for Tc in various kinds of stars (mostly M, S, and C stars) have been performed. Their results are summarized in Table 3 (see also footnote 9).

The important conclusions to be drawn from Table 3 are (i) that *Tc-rich stars are mostly LPVs* (with periods larger than 300 d) and (ii) *the existence of a substantial fraction of Tc-poor S stars and Tc-rich M stars* (Mira Ceti belongs to the latter). The latter group might appear puzzling at first sight, since Tc is not expected to be produced separately from the other s-process elements (hence Tc-rich stars should be of type S rather than M). Detailed s-process calculations in AGB stars [31] show, however, that in some cases Tc becomes detectable in the atmosphere before the M star has turned into an S star, thus making the existence of Tc-rich M stars possible. But conversely, all S stars should then be Tc-rich, making the existence of Tc-poor S stars puzzling in the framework of AGB evolution. To account for Tc-poor S stars, one might in principle imagine situations where successive dredge-ups

[8] Alternative scenarios for the production of Tc—either through spallation reactions at the stellar surface triggered by cosmic-ray protons, or through the photofission of the actinides originally present in the star, triggered by γ-rays from the H-burning shell—have appeared in the literature, but none of these is entirely satisfactory in the context of AGB stars.

[9] Another intercombination line at λ608.523 nm is strongly blended with a Ti I line, and its use is therefore not recommended [3]. This line is used in [7] to derive the frequency of Tc-rich stars among C stars, but this frequency is therefore questionable.

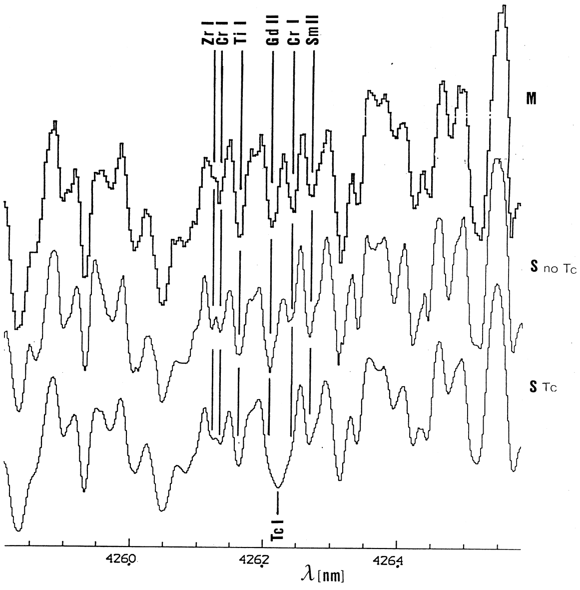

Fig. 10. Comparison of high-resolution spectra of S (lower two thin lines) and M stars (upper thick line) around the Tc I line at λ426.2 nm. The spectra of the two S stars are almost identical, except for the absence of the Tc I line in the upper one. Note that lines from s-process elements are stronger in S stars than in M stars.

are sufficiently far apart that Tc has time to decay below detectable levels before the next dredge-up occurs. S stars might therefore oscillate between the Tc and no-Tc states while evolving on the AGB. Tc-poor S stars exhibit, however, several other properties (like binarity, absence of IR excesses, low luminosities, high $T_{\rm eff}$, and large galactic scale height; see Section 4.1.2) that distinguish them clearly from Tc-rich S stars and that make an oscillation Tc-rich/Tc-poor on the AGB highly unlikely. It is the existence of such a correlation between the absence or presence of Tc and other stellar properties that provides the foundation for the extrinsic/intrinsic paradigm presented in Section 4.1.2.

4.1.2 The Intrinsic/Extrinsic Paradigm for S Stars

The Tc-poor/Tc-rich dichotomy discovered among S stars [67] appears at first sight as quite an innocuous difference that reveals itself on high-resolution spectra only (Figure 10). It hides, however, a very profound difference in the evolutionary status of these two kinds of S stars, and is at the origin of the extrinsic/intrinsic paradigm whose scope goes far beyond the sole family of S stars. This paradigm states that Tc-rich (or "intrinsic") S stars are genuine

Table 3. Surveys of Tc in late-type giants (excluding supergiant stars). $N_{\rm tot}$ refers to the total number of stars in a given sample. The percentage of stars in each given Tc class (certain, probable and possible, doubtful, absent) is listed next. S and M stars have been subdivided into nonvariable or irregular variable stars, and long-period variable (LPV) stars.

	Sample	$N_{\rm tot}$	Tc (%)			no Tc (%)			Ref.
			yes	prob+poss	tot	dbfl	no	tot	
MIII	non var.	17	0	0	0	76	24	100	[67]
	LPV	142	8	28	36	32	32	64	[67]
	All	159			33			67	[67]
S	non var.	16	38	12	50	19	31	50	[67]
	LPV	29	52	31	83	14	3	17	[67]
	All	45			71			29	[67]
	Henize	199	133		66±5	66		34±5	[136]

TP-AGB stars, whereas Tc-poor (or "extrinsic") S stars acquired their chemical peculiarities (namely, carbon and s-process enrichment) through mass transfer across a binary system, at a time when the companion (now a cool WD) was a mass-losing AGB star (see Figure 9). Because the time elapsed since the mass-transfer episode is generally much longer than the half-life of ^{99}Tc, S stars that have been polluted by mass transfer should lack Tc lines. The binary nature of these Tc-poor S stars has indeed been clearly established (Section 4.3.1). But the difference between extrinsic and intrinsic S stars goes beyond the Tc dichotomy: A closer look reveals differences in their average luminosities, effective temperatures, infrared colors, and galactic scale heights, indicative of the different evolutionary stages characterizing the two kinds of S stars (Table 4). The respective properties of intrinsic and extrinsic S stars summarized in Table 4 clearly indicate that intrinsic S stars are low- or intermediate-mass TP-AGB stars, whereas extrinsic S stars are (mainly) low-mass stars either on the RGB or on the E-AGB.

The extrinsic/intrinsic dichotomy is also probably present in C stars, although no definite evidence in that sense has been obtained so far [1]. Besides the 3 Tc-poor C stars uncovered in [67], the only other hint at such a dichotomy among C stars possibly comes from the luminosity function of C stars in the SMC obtained by a deep survey [146]. This luminosity function is characterized by an extended wing of faint C stars, with $M_{\rm bol}$ going down to -1.5 (**Chapter ??**). In fact, this faint tail exactly overlaps the luminosity range covered by extrinsic S stars in the solar neighborhood (Table 4). Whether these faint C stars are actually extrinsic stars would need to be ascertained by specific observations. In any case, this particular example shows that it is important to uncover extrinsic stars in external systems before at-

Table 4. Respective properties of extrinsic and intrinsic S stars (compiled from [52, 54, 136, 138]).

	intrinsic S	extrinsic S
Spectral definition	ZrO bands	
Spectral type	>S3	<S5
Tc	yes	no
Infrared excess at 12 μm	often	never
Mass loss rate ($M_\odot$ yr^{-1})	$>5\times10^{-8}$	$<5\times10^{-8}$
Luminosity	$> L_{\rm 1stTP}$	$< L_{\rm 1stTP}$
$M_{\rm bol}$	-3 to -5.5	-2 to -4
Relative frequency:		
in magnitude-limited sample	$66 \pm 5\%$	$34 \pm 5\%$
in infinite column perpendicular to the galactic plane	$60\,^{+20}_{-50}\,\%$	$40\,^{-20}_{+50}\,\%$
Exponential scale height (pc)	200 ± 100	600 ± 100
Mass ($M_\odot$)	≈ 1.2 to 5	1.5 to 2
Evolutionary stage	TP-AGB	RGB or E-AGB

tempting to derive basic AGB properties like the minimum luminosity for the formation of carbon stars through the third dredge-up (as discussed in **Chapters ?? and ??**).

4.2 The Progeny of Binary AGB stars: The Zoo of Extrinsic, Peculiar Red Stars

This section identifies existing classes of peculiar red stars with the corresponding phase of the binary scenario sketched in Figure 9.

Phases 1 to 6 correspond to the normal evolutionary sequence of low- and intermediate-mass stars and do not require any further discussion here, except for phase 5, which is possibly associated with silicate J-type carbon stars.

4.2.1 Phase 5: Silicate J-Type Carbon Stars?

Several pieces of evidence [2, 154] currently point to the possible binary nature of a puzzling subtype of carbon stars, the J stars which combine a C-rich photosphere with O-rich dust in their circumstellar environment. Arguments suggesting their binary nature include the presence of a circumbinary disk, as inferred from very narrow CO(2-1) lines [55], where the O-rich silicate dust probably resides (a situation encountered in binary post-AGB stars as well; see **Chapter ??**).

Since J stars lack Tc as well as overabundances from other s-process elements, they do not bear the typical signature of mass transfer from a former AGB companion. Hence, if some causal link exists between the (suspected) binary nature of the J stars and their abundance peculiarities (C and Li overabundances, low $^{12}C/^{13}C$ ratios), it may reside in some kind of binary-induced mixing rather than in a mass-transfer episode.

R-type carbon stars are often considered as the progenitors of the more luminous J-type carbon stars, with which they share many abundance similarities. But this evolutionary link is difficult to reconcile with the *total absence* of binary stars among R stars [85]. In a sense, this very unusual circumstance may also possibly hint at a link between binarity and chemical peculiarities for this class of carbon stars (for instance, R stars could all be coalesced binary systems).

4.2.2 Phase 7: Binary Nuclei of PNe (Abell 35-like)

Among PNe with binary nuclei, there is a class consisting of the four objects Abell 35 (BD$-22°$3467 = LW Hya), LoTr 1, LoTr 5 (HD 112313 = IN Com = 2RE J1255+255), and WeBo 1 (=PN G135.6+01.0). Their optical spectra are dominated by late-type (G-K) stars, but the UV spectra reveal the presence of extremely hot ($>10^5$ K), hence young, WD companions. Related systems are HD 128220, consisting of an sdO and a G star in a binary system of period 872 d, and the yellow symbiotic/PN AS 201. In all these cases, the late-type star is chromospherically active and rapidly rotating. This rapid rotation is likely to result from some interaction between the binary components, either during a CE phase (see Section 4.4) or by accretion of spin angular momentum during wind accretion in a detached binary. The long orbital period, known with certainty only for HD 128220, and the similarity with the WIRRing systems described next, favor the latter hypothesis. These systems may thus fit in phase 7 of the binary paradigm, especially WeBo 1 and AS 201, whose late-type components have been shown to be barium stars [12, 102]. There is, however, no definite evidence for s-process overabundances in the other systems [30, 131].

4.2.3 Phase 8: WIRRing Systems (Rapidly Rotating KVBa + Hot WD)

The class of WIRRing stars (wind-induced rapidly rotating) stars was created [49] to describe a small group of rapidly rotating, magnetically active K dwarfs with hot WD companions discovered by the ROSAT Wide Field Camera and *Extreme Ultraviolet Explorer* (EUVE) surveys. From the absence of short-term radial velocity variations, it may be concluded that these systems have periods of a few months at least. Moreover, several arguments, based on proper motion, WD cooling time scale, and lack of photospheric Li, indicate that the rapid rotation of the K dwarf cannot be ascribed to youth. It has been suggested [49] that the K dwarfs in these wide systems were spun up by the accretion of the wind from their companion, when the latter was a mass-losing AGB star. The possibility of accreting a substantial amount of spin from the companion's wind has since been confirmed by *smooth-particle hydrodynamics* simulations of wind accretion in detached binary systems (see Section 3.1 and [130]). A clear signature that mass transfer has been operative in the WIRRing system 2RE J0357+283 is provided by the detection of an overabundance of barium [48]. Interestingly enough, the class of WIRRing stars is not restricted to dwarf primaries, since it probably also includes all yellow symbiotics with dust shells (the so-called d'-type) as well as HD 165141. Those systems share the properties of RS CVn systems and giant barium stars [53, 102]. The very long orbital period of HD 165141 ($P \approx 4800\,\mathrm{d}$) forbids the barium star from having been spun up by tidal effects, as is the case for RS CVn systems. This system, moreover, hosts the hottest WD ($T \approx 35\,000\,\mathrm{K}$) among barium systems. The cooling time scale of the WD is about 10 Myr, shorter than the magnetic braking time scale of the giant star (about 100 Myr) [130]. The mass transfer thus occurred recently enough so that the magnetic braking has not yet slowed down the giant star substantially. HD 165141, WeBo 1, and the yellow d' symbiotics are probably cases in which the mass transfer occurred when the accreting star was already a giant.[10] HD 128220 (G subgiant + sdO companion) may be another example of a subgiant star spun up by the accretion process [42].

4.2.4 Phases 9–10: Dwarf Ba/C Stars, Subgiant CH Stars

Except for those WIRRing stars discussed in the previous section, most extrinsic stars are expected to form as dwarfs, since (i) the stellar lifetime is longer on the main sequence than on the giant branch, and (ii) the cross section for wind accretion is independent of the stellar radius; wind accretion is therefore not less efficient for dwarf accretors than for giant ones (see (11)). About 30 dwarf C stars are known as of this writing (Table 5), and most of them have been uncovered very recently by the *Sloan Digital Sky Survey* [74] and by the *Two Micron All Sky Survey* [72]. Many more may be expected from these surveys in the coming years. Many dC stars appear to have halo kinematics. Their binary nature has not been demonstrated in all cases, but several exhibit the expected barium overabundances.

Dwarf Ba stars (some with C/O > 1) were identified [96] among the stars classified as "FV strong Sr λ4077" in the Michigan spectral survey. The families of CH subgiants [11, 73] and blue metal-poor stars [106] also comprise stars near or slightly above the main sequence. As discussed in Section 4.3.1, these are heterogeneous classes of peculiar stars, merging post-mass-transfer binaries and single stars whose chemical peculiarities are of unknown origin.

[10] It is possible, though, that the giant appearance of the d' symbiotics is a transient phenomenon caused by the accreting dwarf star being driven out of thermal equilibrium by the rapid mass accretion (see Section 4.4.2).

Table 5. Currently known carbon dwarfs and subdwarfs. A + sign in the column labeled Ba indicates that Ba overabundances have been reported.

Name	binary	Pop.	Ba	M_v	discovery paper
PG 0824+289	dCe + DA WD	disk	+	+10.4	[37]
CBS 311 (= SBS 1517+5017)	dC + DA WD	disk	?	+10.8	[66]
KA-2	?	disk	+	>+3.7	[110]
CLS 29?	?	disk	?	?	[133]
0041-295	?	disk?	?		[143]
0045-259	?	halo	?		[143]
G 77-61	yes	halo	+	+10.1	[23]
CLS 31	?	halo	+		[33]
CLS 50	?	halo	+		[32]
CLS 96	?	halo	+		[33]
LHS 1075	?	halo	?		[33]
GD 439	dC + WD	?	?	>+4	[65]
GH 7-21	?	?	?		[64, 145]
SA51-2C24	?	?	+		[16]
2048-348	?	?	?		[143]
LSR 2105+2514	?	?	?		[72]
LP 758-43	?	?	?		[72]
SDSS	17 candidates listed in [72]				[74]

4.2.5 Phase 11: Giant Barium Stars

As indicated in the introduction to Section 4, the mass-transfer scenario was originally introduced [82] to account for the overabundances of barium and other elements produced by the s-process of nucleosynthesis observed at the surface of giant barium stars. Giant barium stars represent about 1% of the giant G-K stars, and this frequency is consistent with the frequency of their "FV strong Sr λ4077" progenitors among FV stars [97]. Early-type CH stars [58], with low $^{12}C/^{13}C$ ratios (of order 10), are the Pop. II analogues of barium stars. The metal-deficient barium stars [73] may also be Pop. II objects but with C/O ratios below unity, in contrast to the situation prevailing for CH stars.

4.2.6 Phase 12: Tc-Poor S or C in Pop. I, Yellow Symbiotics in Pop. II

The identification of Tc-poor S stars as mass-transfer binaries has been discussed at length in Section 4.1.2 and will not be repeated here. This section will instead focus on the relationships between Tc-poor S (or C) stars and various other families of peculiar red stars, namely, barium and symbiotic stars.

The identification of Tc-poor S stars as descendants of the barium stars, first suggested in [47, 67], has now been definitely confirmed on the basis of the similarity of their orbital elements (see Figure 11 and Section 4.3.2).

A more controversial issue concerns the possible relationship between Tc-poor S stars and symbiotic stars, which is raised by the fact that both families consist of mass-losing giants and WD companions in systems with similar orbital periods [137]. This question is actually twofold: **(i) Do symbiotic systems exhibit overabundances of s-process elements? (ii) Do Tc-poor S stars exhibit some symbiotic activity?**

As far as question (i) is concerned, the answer seems negative for "red" symbiotics (i.e., with M giants as primary components), but is positive for "yellow" s-type symbiotics (i.e., with nondusty G or K giants as primary components). In fact, no S stars are known among the giant components of red symbiotics [95], but all yellow s-type symbiotics studied thus far are halo objects exhibiting overabundances of s-process elements [103, 118, 125, 126]. The fact that Pop. II symbiotics involve yellow giants rather than red giants is a likely consequence of the bluer location of the giant branch in low-metallicity populations. In that sense, s-type yellow symbiotics may be seen as the Pop. II analogues of the binary S stars, as both classes populate the upper end of the giant branch.[11] **It is in fact the absence of S stars among red symbiotics that is the real puzzle**. The difference between red symbiotics and Tc-poor S stars resides neither in their orbital parameters nor in their luminosities, as apparent from the similarity between the properties of the M+WD, noneruptive symbiotic systems like SY Mus or RW Hya, and the average Tc-poor S stars. A solution to that puzzle may come instead from the demonstration that red symbiotics actually belong to a more metal-rich population than the binary S stars. Peculiar red giants like carbon and barium stars are indeed known to be rarer in high-metallicity environments (see **Chapter ??** and Section 4.3.1). This scarcity may be a consequence of the less-efficient operation of the s-process at high metallicities with $^{13}C(\alpha,n)^{16}O$ as the neutron source (**Chapter ??**). Conversely, carbon symbiotics are frequent in the low-metallicity environment of the Magellanic Clouds. The suggestion that red symbiotics in the Galaxy may belong to a rather metal-rich population is, however, not borne out by their subsolar carbon abundances [119], despite the claim that their infrared colors may be more typical of metal-rich, bulge M giants than of M giants in the solar neighborhood [150]. A detailed comparison of the kinematics and metallicities of red symbiotics and Tc-poor S stars is necessary to settle this question definitively.

As far as question (ii) is concerned, some Tc-poor S stars indeed exhibit symbiotic activity (Table 6; see also Section 3.1 and [137]), although rather weak in comparison to full-fledged symbiotics. The rarity of the symbiotic phenomenon among extrinsic S stars is fully apparent from the result of a high-

[11] Whether yellow symbiotics belong to phases 4–5 or 12 in Figure 9 cannot be answered at this stage, since the Tc content of these stars is currently unknown.

Table 6. S stars exhibiting symbiotic activity, according to various diagnostics: X-rays (X), UV continuum (in column UV cont., y means that excess UV flux is present, but does not match a clean WD spectrum), C IV $\lambda 155$ nm and Mg II $\lambda 280$ nm lines, Hα emission, and He I $\lambda 1083$ nm. The stars have been ordered according to increasing orbital period. From [137].

Name	P [d]	X	UV cont.	C IV $\lambda 155$	Mg II $\lambda 280$	Hα em.	He I $\lambda 1083$
Hen 108	197	?	?	?	?	no	?
Hen 147	335	?	?	?	?	no	?
HR 1105	596	?	y	y	y	?	var
Hen 137	636	?	?	?	?	moderate	?
HD 35155	642	var?	y	y	y	moderate?	var
Hen 121	764	?	y	?	?	strong	?
HD 191226	1210	?	WD	no	y	?	wk em.
Hen 119	1300	?	?	?	?	no	?
HD 49368	3000	?	y	y	y	no	absorption
HR 363	4590	var	y	no	?	?	wk em.
Hen 18	?	?	y	?	?	strong	?
Hen 134	?	?	?	?	?	moderate	?
ER Del	?	?	?	?	?	strong	?

resolution spectroscopic survey [136, 137] aiming at detecting Hα emission among 40 extrinsic S stars from the Henize sample (see Table 3). It uncovered only 2 stars with strong, broad (FWHM $\approx 70\,\mathrm{km\,s^{-1}}$) and double-peaked H$\alpha$ emission lines resembling the Hα profiles of symbiotic stars. Symbiotic activity in extrinsic S stars seems to be restricted, at least as far as Hα emission is concerned, to the period range 600–1000 d (Table 6), which is also where most red s-type symbiotic stars are found (excluding symbiotic novae and d-type symbiotics hosting Mira variables).

4.2.7 Phase 14: Binary Post-AGB Stars

A detailed description of post-AGB stars is presented in **Chapter ??**. Of interest here are those post-AGB stars residing in binary systems and that in principle fit either in phase 6 (if the companion is a main sequence star) or in phase 14 (if the companion is a WD) of the binary scenario (Figure 9). Unfortunately, the mass functions of these SB1 systems do not always allow one to distinguish between a main-sequence and a WD companion. Most (though not all) binary post-AGB stars are very metal-deficient, and this correlation has been interpreted as the result of reaccretion, from a stable circumbinary disk, of gas depleted in refractory elements (see **Chapter ??** and Section 3.1). The composition of the atmosphere of the binary post-AGB stars does not bear the s-process signature of the third dredge-up, either because the star left the

AGB at an early stage, before these processes had a chance to operate, or as a result of this chemical fractionation (most s-process elements are refractory). Such a chemical fractionation does not seem to be observed in barium stars, despite the fact that these stars are supposed to be the descendants of the binary post-AGB stars in phase 6. At this point, it should be noted, however, that this possibility has never really been investigated in detail. In fact, one cannot totally exclude that the abundance pattern of barium or carbon stars is shaped both by the s-process nucleosynthesis *and* by the refractory properties of the elements (or even in some cases, of their oxides). In that respect, intriguing correlations seem to exist [70] between the abundance patterns observed in carbon stars and in SiC grains found in meteorites, which would clearly deserve further scrutiny. In any case, the apparent incompabitility between the abundances of barium and binary post-AGB stars needs to be properly understood. It is conceivable, for example, that barium stars are not at all the descendants of the binary metal-deficient post-AGB stars, if the latter left the AGB at a very early phase. This possibility is suggested by the similarity of the orbital elements of non-AGB M giants and post-AGB stars observed in Figure 11.

4.3 Orbital Elements of Extrinsic Stars

4.3.1 Binary Statistics of Extrinsic Stars

Field Stars

The results of radial-velocity monitoring aiming at deriving the frequencies of binaries among the various families of extrinsic stars is presented in Table 7. When account is made for various detection biases (due to pole-on or very long period orbits) [54], the fraction of binaries among (disk) subgiant CH stars, "strong" Ba dwarfs (but see below), mild barium stars, strong barium stars, Tc-poor S stars, and CH stars is compatible with 100%. Observed under similar conditions, normal giant stars in the field reveal about 10 to 30% of spectroscopic binaries [86]. This result is especially significant for barium stars with strong anomalies, since the monitored sample includes *all* such stars that are currently known. No similar conclusion can be drawn for dwarf C stars, since there has not been any systematic radial-velocity monitoring for this class of extrinsic stars.

The situation for dwarf barium stars is more confused. On the one hand, the binary frequency in a sample of "strong" Ba dwarfs (including "FV strong λ4077" stars, blue metal-poor stars with Ba overabundances, disk subgiant CH stars, and Ba stars with spectral types earlier than G2 previously classified as giant stars, but which were shown to be dwarfs [98]) is compatible with 100%. But on the other hand, among the 6 barium dwarfs identified by the high-accuracy abundance survey of 200 F dwarfs in the solar neighborhood [26], only HR 4395 is a binary system (with a period of about 2000 d), whereas the other stars clearly have a constant radial-velocity after several years of

Table 7. The fraction of binaries among the various families of extrinsic stars. The column labelled Refs. provides the references where the binary statistics and the orbital elements may be found.

Family	Fraction of binaries	Refs.
dwarf Ba		
"FV str λ4077" and disk CH subgiants	28/30	[84, 98, 99]
blue metal-poor with Ba overabundances	100%?	[106, 127]
Ba dwarfs among FV from [26][a]	1/6	[98, 99]
low-metallicity CH subgiants	0/3	[107]
dwarf C	$\geq$4/31	see Table 5
mild Ba	37/40	[54]
strong Ba	35/37	[54]
Tc-poor S	24/28	[54]
Tc-poor C-N	1/3?	[54]
J	100%?	[154]
CH	>10/12	[87]

[a] The Ba dwarfs are HR 107, HR 2906, HR 4285, HR 4395, HR 5338, HD 6434.

monitoring. This situation is puzzling, since the Ba overabundances (in the range $0.23 \leq [\mathrm{Ba/Fe}] \leq 0.68$) of these barium dwarfs cannot be ascribed to the normal galactic chemical evolution [26]. The situation is similarly puzzling for the *low-metallicity* CH subgiant stars cited in Table 7 that do not exhibit radial-velocity variations despite several years of monitoring.

In summary, binarity indeed appears to be a *necessary* condition to form the classes of peculiar stars listed in Table 7, with the exception of low-metallicity CH subgiants, mild Ba dwarfs, C dwarfs, and Tc-poor C-N stars, for which the situation remains unclear. Whether binarity is a *sufficient* condition to form the barium syndrome has not yet been conclusively answered. There seem indeed to exist giant stars that are *not* barium (or S) stars, although they are components of binary systems with orbital parameters like those of the barium systems. All red symbiotic stars are such cases. Another example is HD 160538 (=DR Dra). A detailed abundance analysis reveals no s-process enhancements whatsoever, while the giant belongs to a binary system with a hot WD companion and $P = 904$ d, $e = 0.07$, typical of barium systems. However, the mass of the WD should be derived to ascertain that its AGB progenitor was massive enough to evolve along the TP-AGB phase and to activate the s-process and the third dredge-up. Other examples that might appear at first sight puzzling are HD 128220 (a rapidly rotating G subgiant and a $0.55 \pm 0.01\,\mathrm{M}_\odot$ sdO star, in a system with $P = 871$ d and $e = 0.21$), HD 185510 (an RS CVn system consisting of a K0III and an sdO star) and HR 1608 (= K0IV + WD with $T_{\rm eff} = 26\,000 \pm 1500$ K) in a system of $P = 903 \pm 5$ d and $e = 0.30 \pm 0.06$. However, the giant star in the latter system need not be a barium star, because the inferred WD mass ($0.40\,^{+0.2}_{-0.15}$ M$_\odot$) is too small for its progenitor to evolve along the TP-AGB (compare this mass with the core masses at the onset of the TP-AGB given in **Chapter ??**). The same holds for the sdO stars in HD 128220 and HD 185510 (about sdO stars, see also **Chapter ??**). Conversely, HD 33959C (F4V + DA), HD 74389 (A2V + DA), and β Crt (A2III-IV + DA) are binary systems with a WD companion discovered recently where the possible barium nature of the primary star would need to be checked.

Globular Clusters

The finding of CH stars in low-concentration globular clusters (like ω Cen, M2, M14, M22, and M55), and not in more concentrated ones [83, 18], provided the first hint that the overabundances of s-process elements observed in chemically peculiar red giants like CH stars were in fact related to binarity [81]. Somehow, binary systems hosting CH stars cannot survive in highly concentrated clusters. The dominant dynamical processes affecting binaries in globular clusters are the disruption of “soft” binaries through stellar encounters and the shrinking of “hard” binaries via energy exchanges with intruder stars. It seems most likely [18] that it is the latter process that accounts for the lack of CH stars in highly concentrated clusters.

In those, the shrinking of “hard” binaries seems efficient enough [18] to drive these binaries to separations (≤ 1 AU) that are too small to accommodate the necessary AGB progenitor of CH systems. This suspicion has been only partially confirmed, since the classical CH stars ROA 55 and ROA 70 in ω Cen have indeed been shown to be binaries [80], but *globular clusters seem to host nonbinary CH, barium, and S stars as well* (M22: [19], ω Cen: [80]). These stars are fainter than the luminosity threshold of the TP-AGB and thus neither internal nucleosynthesis nor mass transfer in a binary system can account for their chemical peculiarities! A scenario specific to globular clusters seems thus at work (see the discussion in [132, 140]).

4.3.2 The $(e, \log P)$ Diagram: Insights into the Mass-Transfer Mode

The $(e, \log P)$ diagram (where e is the eccentricity of the orbit and P its period) allows one to learn much about the evolution followed by a given class of binary systems. First, it shows at a glance the period range spanned by systems of a given family. Second, similarities or dissimilarities between $(e, \log P)$ diagrams of different families allow one to evaluate the likelihood of an evolutionary connection between them. Third, the distribution of eccentricities provides clues to the nature of the mass-transfer process (namely, RLOF versus wind accretion; see also Section 4.4).

Figure 11 compares the $(e, \log P)$ diagrams for the families of binaries described in Section 4.2 along with normal G-KIII stars in open clusters and

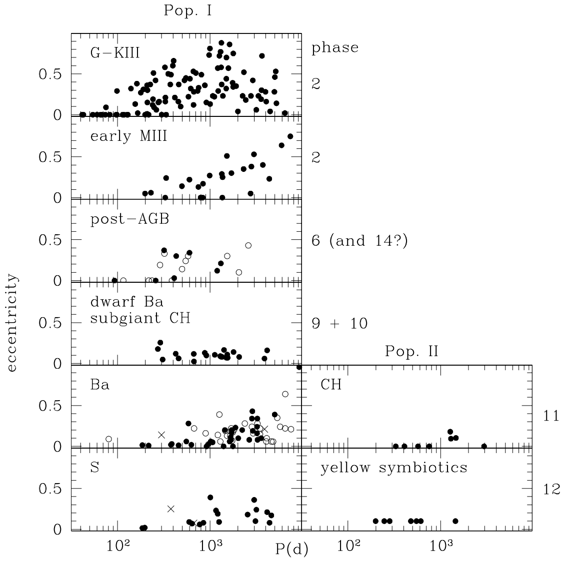

Fig. 11. Comparison of the $(e, \log P)$ diagrams for the families described in Section 4.2, referred to by the phase label of Figure 9 (written to the right of each panel). **Left** and **right** columns correspond to Pop. I and Pop. II systems, respectively. The comparison samples at phase 2 correspond to normal (hence in pre-mass-transfer binaries) G-K giants in open clusters, and to early M giants in the field. Post-AGB systems depleted in refractory elements are represented by black dots; systems not exhibiting the depletion pattern, or with no abundance data, are represented by open dots. The crosses in the Ba panel correspond to the two pairs of the triple system BD+38°118. Ba1,2,3 ("mild" Ba) and Ba4,5 ("strong" Ba) stars are represented by open and filled dots, respectively. In the S panel, crosses correspond to two systems with unusually large mass functions. Since the eccentricities of symbiotic systems are generally poorly determined, they have all been set to 0.1. Orbital elements are taken from the references listed in Table 7, from **Chapter ??** for post-AGB stars, from [88] for normal G-K giants, from [51] for early M giants, and from the references listed by [125] for the yellow symbiotic systems TX CVn, BD−21°3873, LT Del (=He2-467), and AG Dra.

field M giants used as comparison samples of (mostly) pre-mass-transfer binaries. The $(e, \log P)$ diagram of extrinsic systems differs from those of the pre-mass-transfer samples in two clear ways: (i) Many pre-mass-transfer giants are found with $P < 200\,\mathrm{d}$, whereas such short-period systems are quite rare among all extrinsic classes; (ii) the average eccentricity at any given period is much smaller for the extrinsic systems, without being zero, though. These differences between pre-mass-transfer giants and extrinsic systems are a clear indication that the latter have undergone mass transfer and possibly tidal interaction as well. It will be shown in Section 4.4 that the nonzero eccentricities of most of the extrinsic systems argue against Roche lobe overflow (RLOF; Section 2.1) as the mass-transfer mode, since this mode requires the mass-losing star to fill its Roche lobe, a situation where tidal interactions will very rapidly circularize the orbit [142]. Wind accretion is therefore preferred. In that mode, the system remains always detached, and the pollution of the extrinsic star is achieved by the accretion of a fraction of the wind ejected by the companion AGB star (Section 3.1). The requirement that the system have remained always detached seems, however, impossible to satisfy in systems with observed periods as short as 300 d (see Figure 4). RLOF seems thus unavoidable for the short-period systems. That conclusion is troublesome, however, because (i) several short-period systems *are not* in circular orbits (especially among post-AGB and dwarf Ba systems), and (ii) RLOF from an AGB star with a deep convective stellar envelope is generally expected to lead to a CE phase (at least when the mass-losing AGB star is the more massive component), and to a dramatic orbital shrinkage (Section 4.4). The end product of such an evolution is a cataclysmic variable with an orbital period of a few hours, much shorter than the shortest period observed among the extrinsic systems. The very existence of extrinsic systems with periods too short to be accounted for by the wind accretion process indicates that these systems must have avoided the dramatic fate outlined above. Several ways out of this channel (which sometimes does operate, though, since cataclysmic variables *do* exist!) will be sketched in Section 4.4. At this point, it will simply be mentioned that the most detailed simulations of mass transfer available to date for extrinsic systems [56, 104] include prescriptions for wind accretion, RLOF, tidal interaction, and for possibly enhanced mass loss from the AGB star due to the presence of the companion (CRAP, Section 3.3). This last ingredient actually turns out to be an essential one: If a strong mass loss from the AGB star reverses the mass ratio before the onset of RLOF, RLOF will no longer lead to a CE phase nor to dramatic orbital shrinkage (see Figure 14 and Section 4.4). These simulations face, however, two major difficulties (Figure 12): (i) They cannot reproduce the short-period high-eccentricity systems present among extrinsic stars, and (ii) they predict too many extrinsic systems with long periods ($> 10^4$ d). In that respect, it should be stressed that no observational bias alters the period range ($80 < P(\mathrm{d}) \lesssim 10^4$) covered by extrinsic systems (Figure 12), especially for strong barium stars, since the *complete* sample of strong Ba stars has been monitored. Figure 12 therefore reveals that there is both a short- and a long-period cutoff to produce extrinsic systems: If the period is too long, the system is too wide for wind accretion to be efficient and to lead to significant pollution (one example is Mira Ceti itself; Table 1). On the other hand, if the period is too short, another evolutionary channel (leading to cataclysmic variables or to binary sdB stars?) must have been followed [24, 79]. In that respect, it might be interesting to search the primary components of cataclysmic variables for chemical peculiarities similar to those exhibited by extrinsic systems.

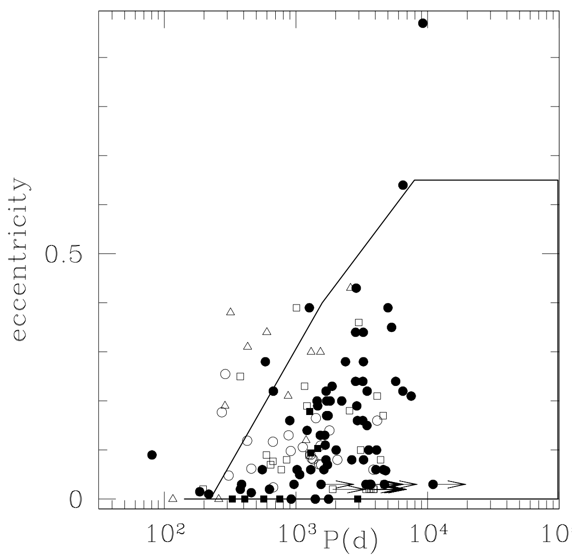

Fig. 12. Comparison of the $(e, \log P)$ diagrams for observed extrinsic systems (filled circles: barium stars; open circles: Ba dwarfs and subgiant CH stars; open triangles: post-AGB stars; open squares: S stars; filled squares: CH stars; arrows mark systems with only a lower limit on their orbital period) and for a synthetic binary population (falling within the thick lines) computed with detailed prescriptions for wind accretion, stable RLOF, and tidal interaction [56]. The displayed synthetic population is that representing the best fit to barium systems, although the model overproduces long-period systems and is unable to account for short-period, high-eccentricity systems observed among post-AGB and dwarf Ba systems.

Finally, Figure 11 fully confirms the hypothesis of an evolutionary link between barium and Tc-poor S stars, which are distributed identically in the $(e, \log P)$ diagram but differ only in terms of their effective temperatures. The same conclusion is reached from the similarity of their mass-function distributions (Section 4.3.3). In contrast, there are dissimilarities between the $(e, \log P)$ diagrams of post-AGB systems, dwarf Ba, and barium stars. If an evolutionary path indeed links these families, physical processes altering the eccentricity and operating specifically in some of these families must be invoked to account for these dissimilarities. For example, tidal circularization of the closest systems ($P < 300\,\mathrm{d}$) may occur when the Ba and S giants ascend the RGB [142]. This process may account for the fact that among the short-period systems, the average eccentricity of giant Ba stars is considerably smaller than that of dwarf Ba systems (Figure 11). Similarly, post-AGB systems with short periods have large eccentricities despite the fact that tidal circularization must have operated during the AGB evolution. The similarity between the $(e, \log P)$ diagrams of post-AGB systems and early M giants might indicate instead that the post-AGB systems did not evolve very far up the AGB. Otherwise, processes driving the eccentricity upwards in post-AGB systems must be invoked, like (i) an exchange of angular momentum between the orbit and the circumbinary disk [5] that frequently occurs in those systems (see Section 3.1 and **Chapter ??**), or (ii) isotropic mass loss occurring preferentially during periastron passages [129].

4.3.3 Comparison of Mass Functions: Insights into the Galactic Population and into the Nature of the Companion

The mass functions of extrinsic systems convey information on the masses of the two components, and hence on the galactic population to which they belong as well as on the nature of the companion (i.e., WD versus main sequence). They may also be used to confirm the evolutionary link between the various families already discussed in Section 4.3.2 in relation to the $(e, \log P)$ diagram. In spectroscopic binaries with only one observable spectrum, as most of the extrinsic systems are, the individual masses are not directly accessible; only the mass function $f(M) = M_2^3 \sin^3 i/(M_1 + M_2)^2$ (where M_1 is the mass of the observable component, M_2 that of the unseen component, and i is the inclination of the orbital plane on the plane of the sky) can be derived directly from the observations. To extract even the mass ratio $Q \equiv M_2^3/(M_1 + M_2)^2$ requires resorting to statistical methods to eliminate the inclination i of the orbital planes, which may be assumed to have their poles distributed randomly on a sphere. Classical inversion methods, like Lucy–Richardson, may be used for that purpose [54] and provide the distribution of Q. The Q distributions of extrinsic systems are typical in that they are quite peaked, contrary to the situation prevailing for normal G-K giants in binary systems (Figure 4.3.3).

The narrow Q distribution typical of extrinsic systems may be seen as the signature of the WD nature of the companions, as required by the binary paradigm sketched in Figure 9. Since Q depends much more sensitively upon M_2 than upon M_1, the narrow range spanned by the WD masses, as observed for field WDs [111], results in a peaked Q distribution for extrinsic systems. In contrast, since the companions of normal giants in binary systems need not be WDs, their masses may span a much wider range (the only proviso being $M_2 \leq M_1$).

Direct detection of the WDs in extrinsic systems by their UV radiation has been achieved in very few cases. Among 15 giant barium stars ever looked at, WD companions have been detected with certainty ([6] and references therein) for ζ Cap, ζ Cyg, 56 Peg, HR 774, HR 4474, HR 5058, HD 104979, and HD 165141 (a tentative detection has been reported for ν^2 Cas, whereas firm or tentative WD detections for HD 65699 and ξ^1 Cet are irrelevant, since these stars are no longer considered to be barium stars). This relatively low success rate may be attributed to the fact that the WD companions are generally very cool ($T_{\mathrm{eff}} < 10^4$ K) and these systems hosting luminous giant stars

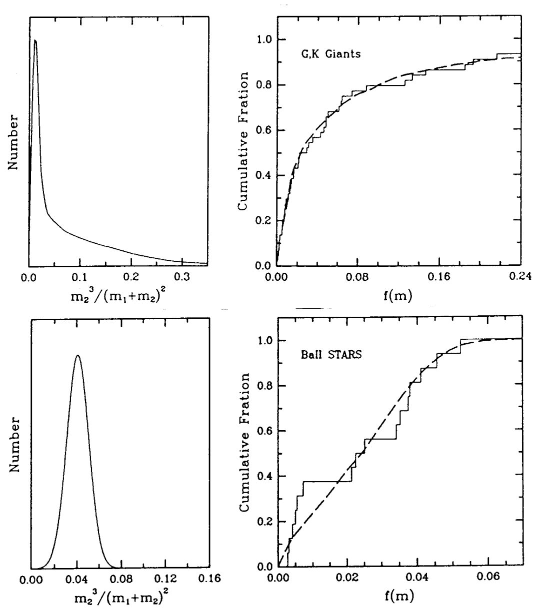

Fig. 13. Comparison of the mass-function (**right panels**) and Q ($\equiv M_2^3/(M_1 + M_2)^2$; **left panels**) distributions of barium stars (**lower panels**) and normal G-K giants (**upper panels**). From [87].

are generally far away. Among 9 Tc-poor S stars that were observed with the *International Ultraviolet Explorer* satellite, only HD 191226 revealed clear signatures of a WD companion (o^1 Ori is another, special, case, since the S star is in fact Tc-rich), whereas a UV continuum has been detected for HR 363, HR 1105, HD 35155, and HD 49368 (Table 6 and references therein). The somewhat larger detection rates may in this case be attributed to the fact that the larger mass-loss rates of S stars as compared to barium giants trigger some kind of symbiotic activity and an associated UV continuum (Section 4.2.6). At this stage, the two puzzling Tc-poor S stars HD 191589 and HDE 332077 should be mentioned. Instead of the WD expected in the framework of the binary paradigm, ultraviolet observations revealed A-type companions, consistent with their outlying mass functions of 0.395 and 1.25 $M_\odot$, respectively. The evolutionary status of these Tc-poor S stars is currently unknown, especially since the current radial-velocity data provide no hint that these systems might be triple.

Direct detection of the WD companion has also been achieved for a few dwarf C stars (see Table 5). A very interesting possibility offered by the Ba dwarfs is a statistical estimate of the mass of their companion (and not just of Q as for the other extrinsic systems). The mass of the Ba dwarf may be derived from a spectroscopic determination of the gravity, effective tempera-

Table 8. Average masses $\overline{M}_1$ of the extrinsic star in the different classes as derived from their $f(M)$ distribution, for two different values of the companion average mass $\overline{M}_2$. N is the number of available orbits.

Family	N	$\overline{Q}$	$\overline{M}_1$		Ref.
			$\overline{M}_2=0.60$	$\overline{M}_2=0.67$	
		[M$_\odot$]	[M$_\odot$]	[M$_\odot$]	
CH	8	0.095	0.9	1.1	[87]
dBa + sgCH	14	0.080	–	1.25±0.25	[99]
Barium (strong)	36	0.049	1.5	1.9	[54]
Barium (mild)	27	0.035	1.9	2.3	[54]
Barium (total)	63	0.043	1.65	2.0	[54]
S (Tc-poor)	17[a]	0.041	1.6	2.0	[54]

[a] The two peculiar S stars HD 191589 and HDE 332077 were not included (see text).

ture, and metallicity combined with a comparison to theoretical evolutionary tracks for given masses. The distribution of the companion masses is then derived by inverse methods from the observed $f(M)$ and inferred primary-mass distributions. The best fit is obtained with a Gaussian distribution for the WD masses centered at 0.67 M$_\odot$ with a dispersion of 0.09 M$_\odot$ [99]. This is the first direct estimate of the average mass of the companion of extrinsic stars. It is in fact close to the average mass of field WDs [111].

Table 8 provides the average Q values and the corresponding masses for various families of extrinsic stars. Masses are derived for two different choices of the average WD mass, namely, $M_2=0.60$ and $0.67\,$M$_\odot$, the latter corresponding to the value directly derived from the analysis of dwarf Ba stars. Barium and Tc-poor S stars have very similar average masses, confirming once again that their different spectroscopic appearance simply results from a difference in their effective temperatures (see also Section 4.3.2), but they belong, in fact, to the same galactic population.[12] As expected, CH stars have an average mass (on the order of $1.1\,$M$_\odot$) that is significantly smaller than that inferred for Ba and S stars (about 1.9–2.3 M$_\odot$, adopting the same average WD mass of 0.67 M$_\odot$ for the three families). This conclusion based on their orbital properties is consistent with the halo kinematics of CH stars. Dwarf barium and subgiant CH stars appear to be intermediate between CH and giant Ba stars. Interestingly enough, these population differences seem to be reflected as well by differences in the corresponding $(e, \log P)$ diagrams (Figure 11), although the interplay between galactic population and orbital dynamics is far from being obvious and still needs to be clarified.

The $f(M)$ distribution of post-AGB binaries is very different from that of the other extrinsic systems. Although some post-AGB systems have mass

[12] A closer look at the $f(M)$ distribution of barium stars [54] reveals that mild barium stars have a slightly larger average mass than strong barium stars (Table 8), a conclusion supported by slightly different kinematic properties [15].

functions similar to those of the other extrinsic families, several have $f(M)$ in the range 0.14–0.97 $M_{\odot}$. This dichotomy confirms that post-AGB binaries are a mixture of systems with main-sequence (phase 6 of Figure 9) and WD (phase 14) companions.

4.4 The Mass-Transfer Mode, or How to Avoid Orbital Shrinkage Due to Unstable RLOF in Extrinsic Systems

This final section is devoted to a discussion of an important problem that arises from the period distribution of all extrinsic systems, as noted in Section 4.3.2 in relation to Figures 11 and 12: These systems that host WD companions have periods in a range that seems incompatible with the standard prescriptions for mass transfer from an AGB star. The observed periods seem too large for being the outcome of dynamically unstable RLOF (resulting in strong orbital decay triggered by a CE phase, and leading to cataclysmic variables) and, at the same time, too short to have been able to host an AGB star in a detached system. The main issue addressed in this section is to identify which one among the various possible mass-transfer modes operated in extrinsic systems: (i) wind accretion in a detached binary; (ii) RLOF in a semidetached system occurring on a dynamical (ii-a) or thermal (ii-b) time scale; (iii) RLOF in a semidetached system occurring on much longer nuclear or orbital time scales. The mass-transfer mode controls the outcome of the process and shapes the post-mass-transfer binary system in several respects:

(a) The efficiency of the *accretion* by the companion star (labeled 1 in the following) of the matter lost by the AGB star (labeled 2) will be high in RLOF modes, which are close to being conservative, i.e., $\mathrm{d}M_1 = -\eta \, \mathrm{d}M_2$ with $\eta \approx 1$. In contrast, in the wind accretion mode, η is on the order of a few percent only [130].

(b) The *reaction of the accreting star* to the matter pouring down upon it will depend on the value of the accretion time scale $M_1/\dot{M}_1$ (which is in turn fixed by the mass-transfer rate, and hence by the mass-transfer mode; Section 4.4.1), as compared to the dynamical and Kelvin–Helmholtz time scales. The catastrophic fate generally associated with RLOF results from the fact that the fast RLOF mass-transfer rates are responsible for short accretion time scales that make the accreting star swell, thus possibly embedding the system in a CE (Section 4.4.2). In turn, this CE exerts a drag on the orbiting stars that may result in a substantial orbital shrinkage.

(c) The RLOF mode is necessarily preceded by a phase of *tidal circularization of the orbit* (Section 4.4.3). Therefore, post-RLOF systems have circular orbits, as opposed to wind-accretion systems where circularization is incomplete.

4.4.1 The Various Mass-Transfer Modes and Associated Stability Criteria

In the framework of the Roche model (Section 2.1), the operation of wind accretion (mode i) as opposed to RLOF (modes ii or iii) is controlled by the ratio $R_2/R_{R,2}$ being smaller than unity, where R_2 is the radius of the mass-losing star and $R_{R,2}$ is the Roche radius (2) around it (in the following, subscripts 2 may be omitted when there is no confusion possible). The RLOF criterion $R_2/R_{R,2} \geq 1$ is in fact too severe for AGB stars, since the scale height of the density stratification in their atmosphere is a significant fraction of their photospheric radius (Section 2.1.3). Therefore, the mass flow through the inner Lagrangian point L_1 becomes nonnegligible long before the photosphere reaches the critical Roche equipotential [101].

Which one among modes (ii-a), (ii-b), or (iii) will operate in a given situation depends on the stability of RLOF mass transfer. The linear stability analysis amounts to a comparison of the first-order variations of the stellar and Roche radii under the effect of mass loss and subsequent orbital evolution:

$$R_2(t_0 + \Delta t) = R_2(t_0) + \frac{\mathrm{d}R_2}{\mathrm{d}M_2}\,\frac{\mathrm{d}M_2}{\mathrm{d}t}\,\Delta t, \tag{12}$$

$$R_R(t_0 + \Delta t) = R_R(t_0) + \frac{\mathrm{d}R_R}{\mathrm{d}M_2}\,\frac{\mathrm{d}M_2}{\mathrm{d}t}\,\Delta t. \tag{13}$$

Stability requires that after mass loss, $\Delta M_2 = \mathrm{d}M_2/\mathrm{d}t\ \Delta t$ (< 0), the star be still contained by its Roche lobe. Assuming that $R_2(t_0) = R_R(t_0)$ is satisfied initially, the stability condition then becomes $R_2(t_0 + \Delta t) \leq R_R(t_0 + \Delta t)$, or $\zeta \geq \zeta_R$, where

$$\zeta_R \equiv \frac{\mathrm{d}\ln R_R}{\mathrm{d}\ln M_2} \tag{14}$$

and

$$\zeta \equiv \frac{\mathrm{d}\ln R_2}{\mathrm{d}\ln M_2}. \tag{15}$$

The radius–mass exponent ζ expresses how the radius of the mass-losing star adapts to a loss of mass. The stability condition simply expresses that if the stellar radius shrinks in response to mass loss ($\zeta > 0$), it must shrink faster than the Roche lobe (hence $\zeta \geq \zeta_R$). A star responds to mass loss on two time scales. The immediate response is (usually[13]) adiabatic. Hydrostatic equilibrium is almost immediately restored, but negligible heat transport occurs on this dynamical time scale τ_{dyn}:

$$\tau_{\mathrm{dyn}} = \left(\frac{R_2^3}{GM_2}\right)^{1/2}, \tag{16}$$

[13] very extended AGB stars, $R \geq 500\ \mathrm{R}_\odot$, with thin envelopes have Kelvin–Helmholtz time scales that become smaller than the dynamical time scales [101].

with G the constant of gravitation. The radius–mass exponent characterizing this adiabatic readjustment is denoted by $\zeta_{\rm ad}$. The star then regains thermal equilibrium by redistributing its internal energy to account for its new distribution of energy sources and mass. This occurs over the Kelvin–Helmholtz time scale $\tau_{\rm KH}$:

$$\tau_{\rm KH} = \frac{G\,M_2\,M_{\rm env}}{R_2\,L_2}, \tag{17}$$

where $M_{\rm env}$ is the envelope mass of the AGB star. The corresponding change in radius is characterized by the exponent $\zeta_{\rm th}$.

The stability condition thus amounts to comparing these responses to the change in the dimension of the star's Roche lobe due to the orbital evolution and the changing mass ratio, and thus can be written $\zeta_R < (\zeta_{\rm th}, \zeta_{\rm ad})$. If this is not satisfied, then mass transfer runs to the fastest unstable time scale.

Adiabatic Radius–Mass Exponent $\zeta_{\rm ad}$ of AGB Stars

The adiabatic radius–mass exponent for (static) AGB stars with a large convective stellar envelope is best represented by that of a condensed polytrope [128], where the central point mass represents the degenerate core (with mass fraction $m = M_{c,2}/M_2$), and the convective envelope is represented by a polytrope of index n ($= \frac{3}{2}$ for a perfect gas, in the absence of radiation pressure). The function $\zeta_{\rm ad} = \zeta(n = \frac{3}{2}; m)$ can be reasonably well fitted (to better than a percent) by the function [128]:

$$\zeta_{\rm ad} = \frac{2m}{3(1-m)} - \frac{1-m}{3(1+2m)} - 0.03\,m + \frac{0.2m}{1+(1-m)^{-6}}\,. \tag{18}$$

For $m = 0$, the above relation yields $\zeta_{\rm ad} = -\frac{1}{3}$, as expected for a polytrope of index $n = \frac{3}{2}$ corresponding to a fully convective star. Thus, *the adiabatic response to mass loss of AGB stars with small core masses ($m < 0.2$) is an increase of their radius* ($\zeta_{\rm ad} < 0$). The adiabatic radius–mass exponent $\zeta_{\rm ad}$ is positive for $m > 0.2$, and goes to infinity as $m \to 1$ (Figure 14). Thus, *AGB stars with large cores ($m > 0.2$) contract as an adiabatic response to mass loss.*

The Thermal Radius–Mass Exponent $\zeta_{\rm th}$ of AGB Stars

The thermal radius–mass exponent $\zeta_{\rm th}$ for AGB stars may be derived from the Stefan–Boltzmann law (expressing that the star is in thermal equilibrium) $L = 4\pi R^2 \sigma_R T_{\rm eff}^4$ (where σ_R is the Stefan–Boltzmann constant), the position of the evolutionary track $L = L(T_{\rm eff}, M)$ in the HR diagram, and the core-mass luminosity relation implying $\partial L/\partial M = 0$. This yields [116]

$$\zeta_{\rm th} \approx -0.3. \tag{19}$$

At this point, it should be stressed that ζ should actually be derived from models including the dynamics of the AGB stellar envelope (**Chapter ??**). A first step in that direction may be found in [115] (equation 12.48), which provides an expression for ζ that includes some properties of dynamical envelopes like the gravitational luminosity and the mass-loss timescale.

The Roche Radius–Mass Exponent ζ_R

The Roche radius–mass exponent ζ_R must be computed by considering how, as a consequence of mass loss $\mathrm{d}M_2$, R_R varies due to variations of the mass ratio and of the orbital separation (or, alternatively, of the orbital angular momentum). Thus, setting $R_{R,2} = Af_2(q)$, where $q = M_2/M_1$,

$$\zeta_R = \frac{\partial \ln R_R}{\partial \ln M_2} = \frac{\mathrm{d}\ln A}{\mathrm{d}\ln M_2} + \frac{\mathrm{d}\ln f_2(q)}{\mathrm{d}\ln q}\frac{\mathrm{d}\ln q}{\mathrm{d}\ln M_2}, \tag{20}$$

where $\mathrm{d}\ln q/\mathrm{d}\ln M_2 = 1 + q\eta$, with $\eta \equiv -\mathrm{d}M_1/\mathrm{d}M_2 \geq 0$ being the accretion rate by the companion star. So-called conservative mass transfer corresponds to $\eta = 1$. The term $\mathrm{d}\ln f_2(q)/\mathrm{d}\ln q$ depends upon the geometry of the Roche lobe. It should be computed for the generalized equipotentials (7) taking into account the extra force driving the mass loss. In the absence of a compact formula for $f_2(q)$ in this general case, (3) will be used instead, but the reader should keep in mind that this treatment thus provides only approximate results. Finally, the term $\mathrm{d}\ln A/\mathrm{d}\ln M_2$ may be rewritten in terms of the changes in the orbital angular momentum J associated with the mass loss/transfer processes. Since

$$J = \left(\frac{GM_1^2M_2^2A}{M_1+M_2}\right)^{1/2}(1-e^2)^{1/2}, \tag{21}$$

it follows that[14]

$$\frac{\mathrm{d}\ln A}{\mathrm{d}\ln M_2} = 2\frac{\mathrm{d}\ln J}{\mathrm{d}\ln M_2} + \frac{q}{1+q}(1-\eta) + 2(\eta q - 1). \tag{22}$$

The term $\mathrm{d}\ln J/\mathrm{d}\ln M_2$ accounts for all possible causes of variations of the orbital angular momentum associated with the mass loss/transfer processes.

Of relevance to the present purpose are the situations where the AGB star loses mass through an isotropic wind, of which a fraction α escapes to infinity, a fraction η is accreted by the companion, and a fraction δ forms a circumbinary ring of radius $A_r = \gamma^2 A$ from which it then escapes to infinity (with $\alpha+\eta+\delta \equiv 1$). Assuming that the AGB star is a point source (thus neglecting magnetic braking), the losses in orbital angular momentum are easily computed by realizing that the escaping matter carries away the specific orbital angular momentum (i.e., per unit mass) h_i at the corresponding location i in the system [128]:

$$\partial J = h_2\,\alpha\,\partial M_2 + h_{\mathrm{ring}}\,\delta\,\partial M_2, \tag{23}$$

[14] Only circular orbits will be considered in the following, since the orbit is supposed to have been circularized by tidal spin-orbit interaction prior to RLOF (Section 4.4.3).

where $h_2 \equiv J_2/M_2 = \frac{1}{1+q}\frac{J}{M_2}$, $h_{\rm ring} = \gamma J/\mu$, and $\mu = M_1 M_2/(M_1 + M_2)$ is the reduced mass of the system (in deriving $h_{\rm ring}$, $\gamma \gg 1$ was assumed). The change in angular momentum thus can be written

$$\partial \ln J = \left(\frac{\alpha}{1+q} + \gamma\, \delta\, (1+q) - \lambda \right) \partial \ln M_2, \tag{24}$$

where the last term accounts for the drag exerted by the escaping wind on the orbital motion (with $\lambda \approx 0.05$ according to the hydrodynamical simulations of [130]). Inserting (22) and (24) into (20) finally yields

$$\zeta_R = 2\left(-\lambda + \frac{1-\eta-\delta}{1+q} + \gamma\delta(1+q)\right) + \frac{q}{1+q}(1-\eta) + 2\eta q - 2 + \frac{\mathrm{d}\ln f_2(q)}{\mathrm{d}\ln q}(1+\eta q)\,. \tag{25}$$

The Roche radius–mass exponent derived from (25) is compared to the adiabatic and thermal radius–mass exponents in Figure 14. Remembering that stable mass transfer corresponds to $\zeta > \zeta_R$, we see that several situations may arise:

(i) *isotropic mass loss from highly non-conservative RLOF ("quasi-wind" accretion).* This case corresponds to the very special circumstance where RLOF is highly nonconservative (i.e., $\eta \ll 1$) and yet leads to isotropic mass loss from the system. Such a situation may perhaps be encountered when the geometry of the Roche equipotential is strongly modified by the extra force driving the mass loss (see Figure 2; remember, however, that the analytical developments presented here are not fully consistent in such situations, since the appropriate $\mathrm{d}\ln f_2(q)/\mathrm{d}\ln q$ term has not been used in (20)). The mass transfer is then dynamically stable, except when $\eta > 0.1$ for massive AGB stars ($M_2 > 3.5\,\mathrm{M}_\odot$). The mass transfer may become thermally unstable for low mass ratios q.

(ii) *quasi-conservative mass transfer.* This situation is either dynamically ($q > 1$) or thermally ($1 > q > 0.7$) unstable, except for small mass ratios $q < 0.7$. A strong wind prior to RLOF may thus stabilize RLOF if it drives q below 0.7.

(iii) *mass loss from a circumbinary ring.* The mass lost from a circumbinary ring carries away a very large amount of orbital angular momentum that makes the Roche radius shrink rapidly, and consequently strongly destabilizes mass transfer.

In summary, according to the above considerations, **RLOF involving an AGB star will be stable in two situations**: (i) The radiation pressure driving the wind opens up the critical Roche equipotential so as to make RLOF highly nonconservative (see the discussion in Section 2.1.2), without storing too much mass in a circumbinary disk, or (ii) RLOF is quasi-conservative, but

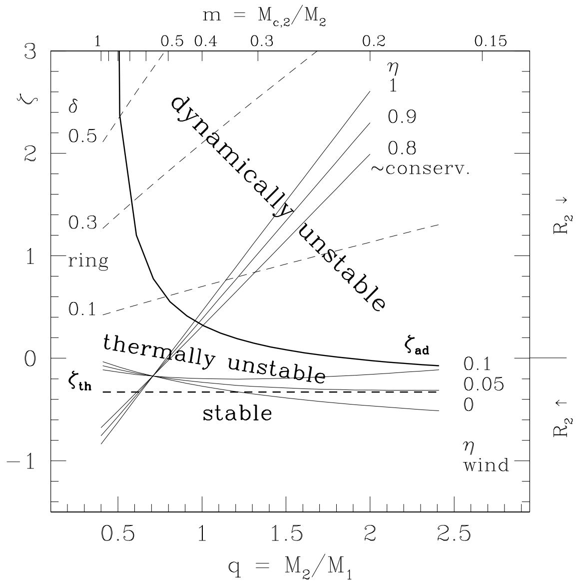

Fig. 14. Comparison of the adiabatic exponent $\zeta_{\rm ad}$ (thick solid line, (18)), thermal exponent $\zeta_{\rm th}$ (thick dashed line; (19)) and Roche exponents ζ_R (thin lines) as a function of the mass ratio M_2/M_1, where M_2 is the mass of the AGB star of relative core mass $m = M_{\rm c,2}/M_2$, and M_1 is the mass of the companion. To fix the ideas, $M_1 = 1.5$ $M_\odot$ and $M_{\rm c,2} = 0.6$ $M_\odot$ have been adopted. The Roche exponent ζ_R has been computed for different mass-transfer modes: isotropic wind with a fraction η ($\ll 1$) accreted by the companion, quasi-conservative evolution ($\eta \approx 1$), and mass loss through a circumbinary ring of radius $\gamma = A_{\rm r}/A = 2$ for a fraction δ of the mass ejected in the wind. The labels along the right-hand vertical axis indicate whether the radius R_2 of the mass-losing AGB star increases or decreases as a result of mass loss.

a former wind episode has reduced the mass ratio below the critical $q = 0.7$ value at the onset of RLOF. However, it should be realized that even though the mass-transfer process does not lead to a runaway, the normal AGB wind mass loss may reach very large values that are comparable to the thermal mass-transfer rates anyway (see **Chapter ??**), so that the reaction of the accreting star is of much concern, even for stable RLOF, as discussed in the next section.

4.4.2 Reaction of the Accreting Star

If RLOF is unstable or if the wind mass-transfer rate is high, the outcome of the mass-transfer process will depend sensitively upon the reaction of the accreting star to the matter being dumped onto it. The worst situation is the one in which a contact system is formed because the accreting star has swollen so much as a reaction to accretion that it has filled its own Roche lobe. The reaction of the accreting star follows the same principles as those describing the reaction to mass loss, except that ΔM_1 is now positive [144]. If the accretion time scale $M_1/\dot{M}_1$ is faster than the Kelvin–Helmholtz time scale of the accreting star, the star cannot regain thermal equilibrium, and its radius evolution will obey the adiabatic exponent $\zeta_{\rm ad,1}$. From considerations based on the run of the specific entropy in the outer layers of stars, it may be concluded [115, 144] that stars with a deep convective stellar envelope have $\zeta_{\rm ad} < 0$ (see Figure 14); hence they contract as a reaction to accretion, whereas stars with radiative envelopes have $\zeta_{\rm ad} > 0$; hence they expand as a result of rapid accretion. Therefore, the risk of forming a contact system does exist only for upper main-sequence companions having radiative envelopes (i.e., $M_1 > 1.2\,{\rm M}_\odot$, as is the case for most of the extrinsic systems but the CH stars; see Table 8). In this case, the instability criterion can be written

$$M_1/\dot{M}_1 < \tau_{\rm HK,1}, \tag{26}$$

or, assuming to fix the ideas that the AGB star loses mass on a thermal time scale and that a fraction η is accreted by the companion,

$$-\frac{M_1}{\eta \dot{M}_2} = \frac{M_1}{M_2}\frac{\tau_{HK,2}}{\eta} < \tau_{\rm KH,1}, \tag{27}$$

or

$$\frac{M_{\rm env,2}}{\eta M_1}\frac{R_1}{R_2}\frac{L_1}{L_2} < 1. \tag{28}$$

This instability criterion is generally largely satisfied (since the mass-losing star 2 is an AGB star, and the accreting star 1 is supposed to be an upper main-sequence star), so that the accreting star will swell. Calculations predict a 10-fold (respectively, 100-fold) increase of the radius of a $2\,{\rm M}_\odot$ star for an accretion rate of 5×10^{-5} ${\rm M}_\odot\,{\rm yr}^{-1}$ (respectively, 2×10^{-4} ${\rm M}_\odot\,{\rm yr}^{-1}$) [59]. These factors are reached already after a few $0.1\,{\rm M}_\odot$ have been accreted. A CE will develop in systems close enough that this radius increase will make the accreting star fill its Roche lobe. This condition has been made more explicit in Table 9, which provides the orbital period below which a common envelope will form for a system consisting of a $3\,{\rm M}_\odot$ AGB star transferring mass onto a $2\,{\rm M}_\odot$ main-sequence companion (in that derivation, an initial radius of $1.7\,{\rm R}_\odot$ is assumed for the main sequence companion, and (2) is adopted for the Roche radius). Since systems involving AGB stars necessarily have periods of a few hundred days, Table 9 reveals that accretion rates larger than about 10^{-4} ${\rm M}_\odot\,{\rm yr}^{-1}$ are needed for a CE to form. The final outcome is, however, uncertain, since such large accretion rates may in fact trigger a strong wind from the accreting star that would then impede accretion, thus preventing the formation of a CE [34]!

Table 9. Critical orbital periods below which a CE forms when a $2\,\mathrm{M}_\odot$ main-sequence star accretes mass from a $3\,\mathrm{M}_\odot$ AGB star at the rate $\dot{M}_{\rm acc}$. The relation between the mass accretion rate and the radius increase $R_{\rm acc}/R_0$ is taken from [59].

$\dot{M}_{\rm acc}$ [$\mathrm{M}_\odot$ yr^{-1}]	$R_{\rm acc}/R_0$	$P_{\rm max}$(CE) [d]
5×10^{-5}	10	18
2×10^{-4}	100	562

At the stage where the two components of the binary system are engulfed by a common gaseous envelope, the CE is generally not corotating with the binary system. As a consequence of the velocity difference between the binary components and the CE, they experience a drag force that works to reduce the binary separation. A large part of the energy deposited into the CE will be in the form of heat, though some fraction will be used to eject the envelope. Although the detailed processes by which the orbital energy is transferred into the CE are complex ones (see [46] and references therein), their global outcome may be encapsulated into the parameter

$$\alpha_{\rm CE} = \frac{\Delta E_{\rm bind}}{\Delta E_{\rm orb}}, \tag{29}$$

describing the efficiency with which orbital energy is used to eject the CE. In that relation, $\Delta E_{\rm bind}$ is the effective binding energy (gravitational minus thermal) of the CE, and $\Delta E_{\rm orb}$ is the variation in the orbital energy of the binary, between the beginning and the end of the process. Assuming that the initial configuration consists of two stars surrounded by a CE of diameter $\approx 2A_0$ (where A_0 is the initial separation), the CE must be ejected from the gravitational field of both components. Under these circumstances, (29) can be written approximately as

$$\frac{(M_1+M_2)(M_2-M_{2,\rm f})}{2A_0} - E_{\rm th} \approx \alpha_{\rm CE}\left(\frac{M_1 M_{2,\rm f}}{2A_{\rm f}} - \frac{M_1 M_2}{2A_0}\right), \tag{30}$$

where the mass of the AGB star varies from M_2 initially to $M_{2,\rm f}$ at the end of the process, and $E_{\rm th}$ is the thermal energy stored in the CE. In spite of the uncertainties involved, the knowledge of $\alpha_{\rm CE}$ coupled with the knowledge of the binding energy of the CE allows one to estimate the final separation of the emerging binary. For AGB stars, several processes are likely to reduce the effective binding energy of the stellar envelope [46] (such as the recombination energy in the hydrogen and helium ionization zones, excitation of nonradial pulsation modes, shock-heating, dust-driven winds, etc.). With those extra energy sources reducing the effective binding energy of the stellar envelope, not so much energy ought to be extracted from the orbit to expel it, thus reducing (and even perhaps suppressing) the orbital decay. As shown in [35], this reduction of the effective binding energy of the AGB stellar envelope by its sole thermal energy is already sufficient to limit the orbital shrinkage to an extent that barium systems like HD 77247 with periods not shorter than 80 d are allowed to form.

In summary, the previous discussion has shown that there are in fact many ways to avoid the dramatic fate usually thought to be associated with RLOF involving AGB stars.

4.4.3 Tidal Interaction and Orbital Circularization

Another important consequence of *any mass-transfer mode involving RLOF* is the tidal circularization of the orbit and the synchronization of the AGB spin with the orbital motion. These two properties result from the fact that as the AGB star comes close to filling its Roche lobe, tides will set in. In general, the stellar envelope cannot adjust instantaneously to the tides because of various sources of viscosity. The tides will therefore not point exactly toward the companion star, which will thus exert a torque on the AGB star. These torques act to synchronize the AGB spin with the orbital motion. Synchronization thus requires the conversion of some spin angular momentum into orbital angular momentum. On the other hand, tides are necessarily accompanied by differential mass motions that will slowly dissipate orbital energy into heat. The gradual lowering of the mechanical energy of the system through this energy dissipation will drive the system closer to its minimum-energy state. For a given mass distribution and fixed total angular momentum, a system has the least mechanical energy when it rotates like a rigid body (e.g., [124]). For a detached binary, this minimum-energy state corresponds to a circular orbit with synchronized spins.

When the orbital angular momentum is much larger than the spin angular momentum, then $\tau_{\rm sync} \propto \left(\frac{A}{R}\right)^6$, whereas $\tau_{\rm circ} \propto \left(\frac{A}{R}\right)^8$, so that synchronization proceeds faster than circularization [45]. Nevertheless, as the AGB star nears its Roche lobe, (R/A) becomes of order unity, and circularization is achieved rapidly. Once a circular orbit has been achieved, it will almost certainly remain circular.[15] Therefore, a post-mass-transfer system with a noncircular orbit has almost certainly not gone through an RLOF phase.

The outcome of the eccentricity in the framework of wind accretion is much more difficult to predict, since it depends on the details of the flow pattern. If the wind is not too much disturbed by the accreting star, and if it is expelled in a spherically symmetric fashion by the synchronously rotating mass-losing star (the so-called Jeans mass-loss mode), the angular momentum in the relative frame attached to the mass-losing star will not change, and so

[15] A process that may turn a circular into an elliptic orbit is a sudden (i.e., occurring on a time scale much smaller than the orbital period) isotropic loss of mass as in supernova explosions, which is probably not relevant here.

the eccentricity will not change [43]. In the case that there is some exchange of momentum between the escaping wind and the accreting star, the eccentricity will change, and its evolution will depend on the flow pattern. Several expressions describing the evolution of the orbital eccentricity in the wind-accretion mode have been proposed in the literature [43, 56, 130]. They correspond to different (inequivalent) parameterizations of the angular momentum transfer. In all cases, the relative eccentricity variation $\Delta e/e$ is found to be proportional to $-\Delta M_1/M_1$; i.e., the eccentricity will decrease in the same proportion as the relative mass increase of the accreting star. This generally does not exceed 10% for wind accretion in a relatively wide binary. Thus, eccentricity variations due to angular momentum transfer during wind accretion remain small. The eccentricity distribution of the barium stars (Figure 11) is satisfactorily reproduced in the framework of the wind accretion scenario, by combining the transfers of angular momentum by wind and tides [56], although those models fail to reproduce the period distribution, as discussed previously in relation to Figure 12.

5 Conclusions and Outlook

This last section provides a list of open questions relating to AGB stars in binary systems:

- The binary paradigm for extrinsic stars is generally well confirmed by current observational data, except for the following questions:
  (i) What is the origin of the seemingly nonbinary Ba dwarfs identified among F dwarfs in the solar neighborhood [26]? The same question applies to the family of low-metallicity subgiant CH stars reported in [107].
  (ii) What is the evolutionary status of the Tc-poor S stars HD 191589 and HDE 332077, which host A-type companions instead of the expected WD?
  (iii) The existence and frequency of extrinsic stars among giant C stars remain to be established.
  (iv) Is binarity a sufficient condition to form, e.g., barium systems, or in other words, are there *normal* (non-barium) giants in binary systems with a WD companion massive enough (i.e., ≥ 0.6 $M_\odot$) for its progenitor to have gone through the TP-AGB phase? If so, what is the other parameter besides binarity needed to form barium stars (e.g., low metallicity)? In a sense, this is an indirect way to identify the conditions required for the s-process and the third dredge-up to operate in AGB stars.
- The puzzling suggestion arising from the analysis of MACHO light curves [152] that 25% of all AGB stars in the LMC belong to semidetached binaries should be further explored.

- More hydrodynamic simulations exploring the parameter space characterizing wind mass-loss from AGB stars in binary systems should be performed to better characterize the different regimes leading to the various possible flow structures (spiral arm, bipolar nebula, circumbinary disk, inner Lagrangian point stream) developing in those binary systems.
- The link between symbiotic stars and extrinsic stars remains to be clarified, and in particular, why red symbiotic stars never exhibit overabundances of s-process elements. A possible hint could come from a kinematic or metallicity analysis of red symbiotic stars to assess whether they belong to a more metal-rich population than Tc-poor S stars do. Another open question relating to symbiotic stars is to identify the parameter(s) controlling their symbiotic activity, not shared by Tc-poor S stars, and explaining why the latter stars exhibit only weak symbiotic activity despite orbital elements identical to those of full-fledged symbiotics.
- Why does chemical fractionation operate in binary post-AGB stars, but leaves (apparently) no signature in their progeny (the barium and Tc-poor S stars)?
- If some cataclysmic variables indeed result from the same evolutionary channels as those producing extrinsic stars (except that RLOF is dynamically unstable in the former case), a search for heavy-element overabundances in the primaries of CVs might prove successful.
- If the $(e, \log P)$ diagrams of binary systems belonging to different galactic populations are indeed significantly different (typically, binaries involving older, or, equivalently, less massive, stars seem to have lower eccentricities on average at any given period), the origin of this interplay between galactic population and orbital dynamics should be clarified. In other words, synthesis of binary populations as in [56] should include metallicity as a parameter impacting on, e.g., the AGB radius and the mass loss rate. These improved models should also aim at properly reproducing the period distribution of barium stars. This requires a careful assessment of the RLOF stability, in order to avoid dynamical RLOF and dramatic orbital shrinkage. This assessment in turn requires the evaluation of the adiabatic and thermal radius–mass exponents in a fully dynamical AGB model (including pulsation and mass loss). The possibly stabilizing effect of a wind from the accreting star, and of the modified Roche geometry in the presence of a radiation-driven wind from the mass-losing star, should also be properly evaluated.
- An evaluation of the consequences of a possible coupling between the AGB pulsation and the dynamical tides raised by the companion would be of interest.

References

1. Abia, C., Domínguez, I., Gallino, R., et al. *ApJ*, 579, 817, 2002.

2. Abia, C. and Isern, J. *ApJ*, 536, 438, 2000.
3. Abia, C. and Wallerstein, G. *MNRAS*, 293, 89, 1998.
4. Alvarez, R., Jorissen, A., Plez, B., et al. *A&A*, 379, 305, 2001.
5. Artymowicz, P., Clarke, C. J., Lubow, S. H., and Pringle, J. E. *ApJ*, 370, L35, 1991.
6. Böhm-Vitense, E., Carpenter, K., Robinson, R., Ake, T., and Brown, J. *ApJ*, 533, 969, 2000.
7. Barnbaum, C. and Morris, M. *BAAS*, 182, #4617, 1993.
8. Batten, A. H., Fletcher, J. M., and McCarthy, D. G. *Publ. DAO*, 17, 1, 1989.
9. Belczyński, K., Mikołajewska, J., Munari, U., Ivison, R. J., and Friedjung, M. *PASP*, 146, 407, 2000.
10. Bolton, C. T. *ApJ*, 200, 269, 1975.
11. Bond, H. E. *ApJ*, 194, 95, 1974.
12. Bond, H. E., Pollacco, D. L., and Webbink, R. F. *AJ*, 125, 260, 2003.
13. Bondi, H. and Hoyle, F. *MNRAS*, 104, 273, 1944.
14. Carpenter, K. G. In Kondo, Y., Sisteró, R. F., and Polidan, R. S., editors, *Evolutionary Processes in Interacting Binary Stars (IAU Symp. 151)*, page 51, Dordrecht, 1992. Kluwer.
15. Catchpole, R. M., Robertson, B. S. C., and Warren, P. R. *MNRAS*, 181, 391, 1977.
16. Chiu, L.-T. G. and Kron, R. G. *Nature*, 299, 702, 1982.
17. Corradi, R. L. M., Ferrer, O. E., Schwarz, H. E., Brandi, E., and García, L. *A&A*, 348, 978, 1999.
18. Côté, P., Hanes, D. A., McLaughlin, D. E., et al. *ApJ*, 476, L15, 1997.
19. Côté, P., Pryor, C., McClure, R. D., Fletcher, J. M., and Hesser, J. E. *AJ*, 112, 574, 1996.
20. Cowling, T. G. *MNRAS*, 101, 367, 1941.
21. Crowther, P. A. *MNRAS*, 290, L59, 1997.
22. Cruzalebes, P., Lopez, B., Bester, M., Gendron, E., and Sams, B. *A&A*, 338, 132, 1998.
23. Dahn, C. C., Liebert, J., Kron, R. G., Spinrad, H., and Hintzen, P. M. *ApJ*, 216, 757, 1977.
24. de Kool, M. and Ritter, H. *A&A*, 267, 397, 1993.
25. Dumm, T. and Schild, H. *New Astr.*, 3, 137, 1998.
26. Edvardsson, B., Andersen, J., Gustafsson, B., et al. *A&A*, 275, 101, 1993.
27. Folini, D. and Walder, R. *Ap&SS*, 274, 189, 2000.
28. Frankowski, A. and Tylenda, R. *A&A*, 367, 513, 2001.
29. Gális, R., Hric, L., Friedjung, M., and Petrík, K. *A&A*, 348, 533, 1999.
30. Gatti, A. A., Drew, J. E., Lumsden, S., et al. In *Planetary Nebulae (IAU Symp. 180)*, volume 180, page 105, 1997.
31. Goriely, S. and Mowlavi, N. *A&A*, 362, 599, 2000.
32. Green, P. J., Margon, B., Anderson, S. F., and MacConnell, D. J. *ApJ*, 400, 659, 1992.
33. Green, P. J., Margon, B., and MacConnell, D. J. *ApJ*, 380, L31, 1991.
34. Hachisu, I., Kato, M., and Nomoto, K. *ApJ*, 470, L97, 1996.
35. Han, Z., Eggleton, P. P., Podsiadlowski, P., and Tout, C. A. *MNRAS*, 277, 1443, 1995.
36. Haniff, C. A., Scholz, M., and Tuthill, P. G. *MNRAS*, 276, 640, 1995.
37. Heber, U., Bade, N., Jordan, S., and Voges, W. *A&A*, 267, L31, 1993.

38. Herbig, G. H. *Kleine Veröff. Remeis-Sternwarte*, 4, No 40, 164, 1965.
39. Herman, J. and Habing, H. J. *Phys. Rep.*, 124, 255, 1985.
40. Hinkle, K., Lebzelter, T., Joyce, R., and Fekel, F. *ApJ*, 123, 1002, 2002.
41. Hinkle, K. H., Lebzelter, T., and Scharlach, W. W. G. *AJ*, 114, 2686, 1997.
42. Howarth, I. D. and Heber, U. *PASP*, 102, 912, 1990.
43. Huang, S. S. *AJ*, 61, 49, 1956.
44. Hünsch, M., Schmitt, J. H. M. M., Schröder, K., and Zickgraf, F. *A&A*, 330, 225, 1998.
45. Hut, P. *A&A*, 99, 126, 1981.
46. Iben, Jr, I. and Livio, M. *PASP*, 105, 1373, 1993.
47. Iben, Jr, I. and Renzini, A. *ARA&A*, 21, 271, 1983.
48. Jeffries, R. D. and Smalley, B. *A&A*, 315, L19, 1996.
49. Jeffries, R. D. and Stevens, I. R. *MNRAS*, 279, 180, 1996.
50. Jorissen, A. In Sterken, C. and de Groot, M., editors, *The Impact of Long-Term Monitoring on Variable Star Research*, page 143, Dordrecht, 1994. Kluwer.
51. Jorissen, A., Famaey, B., Dedecker, M., et al. *Rev. Mex. Astron. Astrophys.*, in press, 2003.
52. Jorissen, A. and Knapp, G. R. *A&A*, 129, 363, 1998.
53. Jorissen, A., Schmitt, J. H. M. M., Carquillat, J. M., Ginestet, N., and Bickert, K. F. *A&A*, 306, 467, 1996.
54. Jorissen, A., Van Eck, S., Mayor, M., and Udry, S. *A&A*, 332, 877, 1998.
55. Jura, M. and Kahane, C. *ApJ*, 521, 302, 1999.
56. Karakas, A. I., Tout, C. A., and Lattanzio, J. C. *MNRAS*, 316, 689, 2000.
57. Karovska, M., Hack, W., Raymond, J., and Guinan, E. *ApJ*, 482, L175, 1997.
58. Keenan, P. C. *PASP*, 105, 905, 1993.
59. Kippenhahn, R. and Meyer-Hofmeister, E. *A&A*, 54, 539, 1977.
60. Knapp, G. R., Dobrovolsky, S. I., Ivezić , Z., et al. *A&A*, 351, 97, 1999.
61. Knapp, G. R., Young, K., and Crosas, M. *A&A*, 346, 175, 1999.
62. Kondo, Y., McCluskey, G. E. J., and Gulden, S. L. In Boldt, E. and Kondo, Y., editors, *X-Ray Binaries (NASA SP-389)*, page 499, Washington D.C., 1976. NASA.
63. Lewis, B. M., Eder, J., and Terzian, Y. *AJ*, 94, 1025, 1987.
64. Liebert, J. *ApJ*, 204, L93, 1976.
65. Liebert, J., Dahn, C. C., Gresham, M., and Strittmatter, P. A. *ApJ*, 233, 226, 1979.
66. Liebert, J., Schmidt, G. D., Lesser, M., et al. *ApJ*, 421, 733, 1994.
67. Little, S. J., Little-Marenin, I. R., and Bauer, W. H. *AJ*, 94, 981, 1987.
68. Livio, M. In Shore, S. N., Livio, M., and van den Heuvel, E. P. J., editors, *Interacting Binaries (Saas-Fee Advanced Course 22)*, page 135, Berlin, 1994. Springer-Verlag.
69. Livio, M. and Soker, N. *ApJ*, 552, 685, 2001.
70. Lodders, K. and Fegley, B. J. *ApJ*, 484, L71, 1997.
71. Lopez, B., Danchi, W. C., Bester, M., et al. *ApJ*, 488, 807, 1997.
72. Lowrance, P. J., Kirkpatrick, J. D., Reid, I. N., Cruz, K. L., and Liebert, J. *ApJ*, 584, L95, 2003.
73. Luck, R. E. and Bond, H. E. *ApJS*, 77, 515, 1991.
74. Margon, B., Anderson, S. F., Harris, H. C., et al. *AJ*, 124, 1651, 2002.
75. Mason, B. D. *AJ*, 112, 2260, 1996.
76. Mason, B. D., Martin, C., Hartkopf, W. I., et al. *AJ*, 117, 1890, 1999.

77. Mastrodemos, N. and Morris, M. *ApJ*, 497, 303, 1998.
78. Mastrodemos, N. and Morris, M. *ApJ*, 523, 357, 1999.
79. Maxted, P. F. L., Heber, U., Marsh, T. R., and North, R. C. *MNRAS*, 326, 1391, 2001.
80. Mayor, M., Meylan, G., Udry, S., et al. *AJ*, 114, 1087, 1997.
81. McClure, R. D. *Mem. Soc. Astron. Italiana*, 50, 15, 1979.
82. McClure, R. D. *PASP*, 96, 117, 1984.
83. McClure, R. D. *ApJ*, 280, L31, 1984.
84. McClure, R. D. *PASP*, 109, 536, 1997.
85. McClure, R. D. *PASP*, 109, 256, 1997.
86. McClure, R. D., Fletcher, J. M., and Nemec, J. M. *ApJ*, 238, L35, 1980.
87. McClure, R. D. and Woodsworth, A. W. *ApJ*, 352, 709, 1990.
88. Mermilliod, J.-C. In Milone, E. and Mermilliod, J.-C., editors, *The Origins, Evolution, and Destinies of Binary Stars in Clusters*, ASP Conf. Ser. 90, page 95. Astron. Soc. Pacific, 1996.
89. Merrill, P. W. *ApJ*, 116, 21, 1952.
90. Merrill, P. W. *Science*, 115, 484, 1952.
91. Merrill, P. W. *PASP*, 68, 162, 1956.
92. Mikołajewska, J. In Mikołajewska, J., editor, *Physical Processes in Symbiotic Binaries and Related Systems*, page 3, Warsaw, 1997. Copernicus Foundation for Polish Astronomy.
93. Morris, M. *PASP*, 99, 1115, 1987.
94. Munari, U. and Whitelock, P. A. *MNRAS*, 237, 45P, 1989.
95. Mürset, U. and Schmid, H. M. *A&AS*, 137, 473, 1999.
96. North, P., Berthet, S., and Lanz, T. *A&A*, 281, 775, 1994.
97. North, P. and Duquennoy, A. *A&A*, 244, 335, 1991.
98. North, P. and Duquennoy, A. In Duquennoy, A. and Mayor, M., editors, *Binaries as Tracers of Stellar Formation*, page 202, Cambridge, 1992. Cambridge University Press.
99. North, P., Jorissen, A., and Mayor, M. In Wing, R. F., editor, *The Carbon Star Phenomenon (IAU Symp. 177)*, page 269, Dordrecht, 2000. Kluwer.
100. Osterbart, R., Langer, N., and Weigelt, G. *A&A*, 325, 609, 1997.
101. Pastetter, L. and Ritter, H. *A&A*, 214, 186, 1989.
102. Pereira, C. B., Cunha, K., and Smith, V. V. In Corradi, R., Mikołajewska, J., and Mahoney, T. J., editors, *Symbiotic stars probing stellar evolution*, Astron. Soc. Pacific Conf. Ser., in press, San Francisco, 2003. Astron. Soc. Pacific.
103. Pereira, C. B., Smith, V. V., and Cunha, K. *AJ*, 116, 1977, 1998.
104. Pols, O., Karakas, A. I., Lattanzio, J. C., and Tout, C. A. In Corradi, R., Mikołajewska, J., and Mahoney, T. J., editors, *Symbiotic Stars Probing Stellar Evolution*, Astron. Soc. Pacific Conf. Ser., in press, San Francisco, 2003. Astron. Soc. Pacific.
105. Pourbaix, D., Platais, I., Detournay, S., et al. *A&A*, 399, 1167, 2003.
106. Preston, G. W. and Sneden, C. *AJ*, 120, 1014, 2000.
107. Preston, G. W. and Sneden, C. *AJ*, 122, 1545, 2001.
108. Prieur, J. L., Aristidi, E., Lopez, B., et al. *ApJS*, 139, 249, 2002.
109. Proust, D., Ochsenbein, F., and Pettersen, B. R. *A&AS*, 44, 179, 1981.
110. Ratnatunga, J. PhD thesis, Australian National Observatory, 1983.
111. Reid, I. N. *AJ*, 111, 2000, 1996.
112. Reimers, D. and Cassatella, A. *ApJ*, 297, 275, 1985.

113. Richichi, A., Baffa, C., Calamai, G., and Lisi, F. *AJ*, 112, 2786, 1996.
114. Richichi, A., Calamai, G., and Stecklum, B. *A&A*, 382, 178, 2002.
115. Ritter, H. In Wijers, R. A. M. J., Davies, M. B., and Tout, C. A., editors, *Evolutionary Processes in Binary Stars*, page 223, Dordrecht, 1996. Kluwer.
116. Ritter, H. *MNRAS*, 309, 360, 1999.
117. Sahai, R. *A&A*, 253, L33, 1992.
118. Schmid, H. M. *A&A*, 284, 156, 1994.
119. Schmidt, M. and Mikołajewska, J. In Corradi, R. and Mikołajewska, J., editors, *Symbiotic stars probing stellar evolution*, Astron. Soc. Pacific Conf. Ser., in press, San Francisco, 2003. Astron. Soc. Pacific.
120. Schuerman, D. W. *Ap&SS*, 19, 351, 1972.
121. Schwarz, H. E., Nyman, L.-A., Seaquist, E. R., and Ivison, R. J. *A&A*, 303, 833, 1995.
122. Shcherbakov, A. G. and Tuominen, I. *A&A*, 255, 215, 1992.
123. Shore, S. N. In Shore, S. N., Livio, M., and van den Heuvel, E., editors, *Interacting Binaries (Saas-Fee Advanced Course 22)*, page 1, Berlin, 1994. Springer-Verlag.
124. Shu, F. H. and Lubow, S. H. *ARA&A*, 19, 277, 1981.
125. Smith, V. V., Cunha, K., Jorissen, A., and Boffin, H. M. J. *A&A*, 315, 179, 1996.
126. Smith, V. V., Cunha, K., Jorissen, A., and Boffin, H. M. J. *A&A*, 324, 97, 1997.
127. Sneden, C., Preston, G. W., and Cowan, J. J. *AJ*, in press (astro-ph/0304064), 2003.
128. Soberman, G. E., Phinney, E. S., and van den Heuvel, E. P. J. *A&A*, 327, 620, 1997.
129. Soker, N. *A&A*, 357, 557, 2000.
130. Theuns, T., Boffin, H. M. J., and Jorissen, A. *MNRAS*, 280, 1264, 1996.
131. Thevenin, F. and Jasniewicz, G. *A&A*, 320, 913, 1997.
132. Thoul, A., Jorissen, A., Goriely, S., et al. *A&A*, 383, 491, 2002.
133. Totten, E. J., Irwin, M. J., and Whitelock, P. A. *MNRAS*, 314, 630, 2000.
134. Tout, C. A. and Eggleton, P. P. *MNRAS*, 231, 823, 1988.
135. Udry, S., Jorissen, A., Mayor, M., and Van Eck, S. *A&AS*, 131, 25, 1998.
136. Van Eck, S. and Jorissen, A. *A&A*, 360, 196, 2000.
137. Van Eck, S. and Jorissen, A. *A&A*, 396, 599, 2002.
138. Van Eck, S., Jorissen, A., Udry, S., Mayor, M., and Pernier, B. *A&A*, 329, 971, 1998.
139. Van Leeuwen, F., Feast, M. W., Whitelock, P. A., and Yudin, B. *MNRAS*, 287, 955, 1997.
140. Vanture, A. D., Wallerstein, G., and Suntzeff, N. B. *ApJ*, 569, 984, 2002.
141. Vardya, M. S. *A&AS*, 73, 181, 1988.
142. Verbunt, F. and Phinney, E. S. *A&A*, 296, 709, 1995.
143. Warren, S. J., Irwin, M. J., Evans, D. W., et al. *MNRAS*, 261, 185, 1993.
144. Webbink, R. F. In Pringle, J. E. and Wade, R. A., editors, *Interacting Binary Stars*, page 39, Cambridge, 1985. Cambridge University Press.
145. Wegner, G. *MNRAS*, 171, 529, 1975.
146. Westerlund, B. E., Azzopardi, M., Breysacher, J., and Rebeirot, E. *A&A*, 303, 107, 1995.
147. Whitelock, P. A. *PASP*, 99, 573, 1987.

148. Whitelock, P. A. In Tateuki, M. and Sasselov, D., editors, *Pulsating Stars: Recent Developments in Theory and Observation*, page 31. Academic Press, 1998.
149. Whitelock, P. A. and Feast, M. *MNRAS*, 319, 759, 2000.
150. Whitelock, P. A. and Munari, U. *A&A*, 255, 171, 1992.
151. Willems, B. and Aerts, C. *A&A*, 384, 441, 2002.
152. Wood, P. R. *Publ. Astron. Soc. Australia*, 17, 18, 2000.
153. Wood, P. R. and Sebo, K. M. *MNRAS*, 282, 958, 1996.
154. Yamamura, I., Dominik, C., de Jong, T., Waters, L. B. F. M., and Molster, F. J. *A&A*, 363, 629, 2000.